Simulating gait with the 3R60 knee prosthesis and a control moment gyroscope

Nathan Timmers

Master of Science Thesis

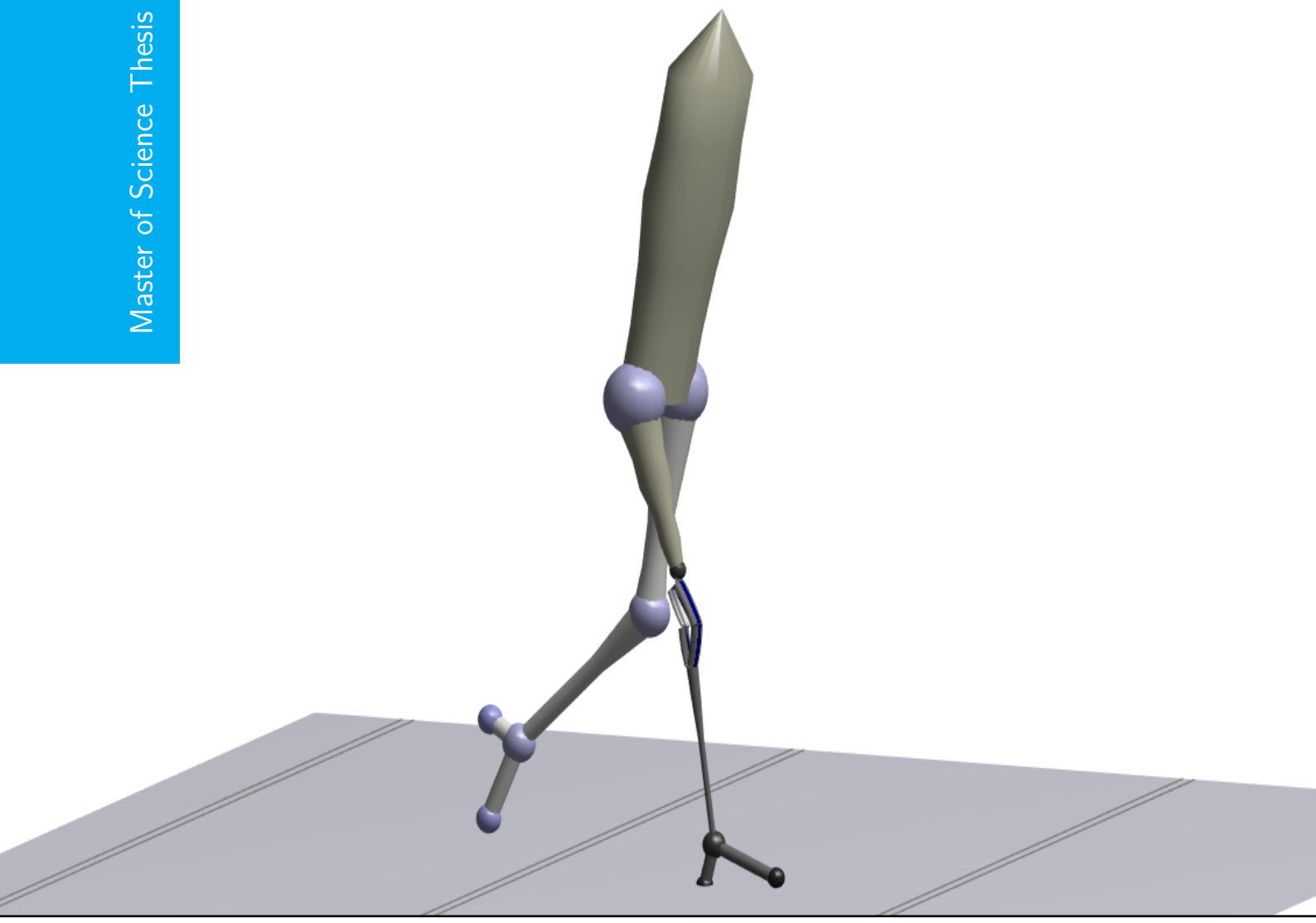

TU Delft Delft University of Technology

Delft Center for Systems and Control

Simulating gait with the 3R60 knee prosthesis and a control moment gyroscope

Master of Science Thesis

For the degree of Master of Science in Systems and Control, and Mechanical Engineering at Delft University of Technology

Nathan Timmers

December 15, 2020

Thesis committee:	Prof. Dr.-Ing. H. Vallery	TU Delft	Supervisor
	Dr.-Ing. J. Kober	TU Delft	Supervisor
	ir. S. Jabeen	TU Delft	Daily supervisor
	Dr. ir. G. Smit	TU Delft	External committee member

Faculty of Mechanical, Maritime and Materials Engineering (3mE) · Delft University of Technology

Table of Contents

List of Figures

List of Tables

Preface

Ending an era, that is how graduating feels. Luckily I could graduate on a topic that lies within my interests. After having done a gap year by joining the Project March dreamteam, I found out that technology in combination with humans is something I find interesting. Especially the field of rehabilitation. The thesis project has made me learn more about simulation, amputee gait, prostheses, and numerical challenges that arise during simulation. Although the thesis project started out with a different goal, in the end I am happy with the resulting goal and results. Of course I hope that it can be of great use for further research and it will be interesting to see what the new findings will be.

There are several people who I want to thank. Without them I would not stand where I am today. First of all, I want to thank my lovely wife Mirte. I am thankful for your love and support that you have shown. This year has given me many reasons to celebrate, since we got married this summer, the same year that I am graduating. I want to thank my parents Gert Jan and Bea, who have supported me massively from the very beginning that I started studying. The fact that I was able to join C.S.R., Project March, while you continued supporting me has contributed in developing myself and knowing more about my interests. Lastly, I want to thank God, who has guided me throughout my life.

Simulating gait with the 3R60 knee prosthesis and a control moment gyroscope

Nathan Timmers

***Abstract*— Developing a new knee prosthesis requires thorough testing. Forward dynamics simulation can be valuable in the development process. It can reduce the need for intermediate prototypes and tests. Currently, there are 3D simulations of healthy walking and kinematic models of common prosthesis like the 3R60. However, they have not yet been combined. Such a model could function as a baseline for newly developed prostheses. It would also open possibilities for researchers to modify the prosthesis design by analyzing different scenarios in simulations. In this paper an existing 3D neuromuscular model of a healthy human is adjusted so that it represents a trans-femoral amputee with a 3R60. The model is simulated walking with an average velocity of $0.9\,\mathrm{m/s}$ and $1.2\,\mathrm{m/s}$. The performance of the model is evaluated by comparing gait differences between the healthy and amputee model to findings from literature. The simulated amputee gait agrees well with literature, especially for a velocity of $1.2\,\mathrm{m/s}$. When walking $0.9\,\mathrm{m/s}$ the model oscillates in the coronal plane, suggesting it has difficulty maintaining balance. Furthermore, a case study was done on fall prevention using a control moment gyroscope embedded in the prosthetic shank. The control moment gyroscope increases the ability to flex and extend the prosthetic knee, which can help with fall prevention. With the added control moment gyroscope the gait at $1.2\,\mathrm{m/s}$ became more symmetric. A fall was prevented after a trip using a control moment gyroscope, however, this simulation is numerically too sensitive to draw conclusions.**

***Index Terms*— Control moment gyroscope, fall prevention, gait simulation, neuromuscular model, trans-femoral amputee**

I. Introduction

IT was estimated that in the United States in 2005 around 623,000 people were living with an trans-femoral (TF), also called above-knee (AK), amputation and it is predicted that this may double by the year 2050 [1]. There exist knee prostheses that help overcoming the loss of knee, such the Ossur Rheo Knee, or the Otto Bock C-leg [2]. However, these devices do not mimic the natural knee perfectly. This results in several challenges the TF amputees face, such as increased energy expenditure compared to healthy people [3]–[5]. Also the amputee gait is characterized by being asymmetric, which can develop negative changes in the joints of the intact limb such as osteoarthritis [6]. Furthermore, TF amputees have less control over their knee which makes it harder to prevent falling after trips and slips [7], [8]. In several recent studies researches presented newly developed knee prostheses, with the purpose of improving the quality of prostheses [9]–[14]. All newly developed knee prostheses need validation through experiments in order to evaluate their real performance. This requires multiple participants and an expert on prosthetic alignment. Ideally, the experiment is only used for the final evaluation. However, time is needed for tuning the new device and for participants to get used to the device. This may be an iterative process. Executing an initial evaluation of prostheses via forward dynamic (FD) simulation can be valuable in these situations. It can be executed at any time, and it can be used to compare different scenarios, such as control algorithms, for rough tuning. This reduces the need to build different prototypes, and the need to use participants for intermediate tests.

Multiple studies have used FD simulation to evaluate a new knee prosthesis [9]–[11], [13], [15]. Most of these studies compare the results from simulation to data of healthy people, which seems logical as one would want the resulting gait to mimic the gait of healthy people. However, there are several shortcomings to the methods that were used. Several studies use an optimal torque generator to drive the joints of the model. This generates a torque such that it minimizes the error between simulated and desired joint angles [9]–[11], [15]. This modeling approach does not take the physiological limitations of a human into account, because muscles cannot generate instant and infinite amount of torque. The model of Thatte and Geyer [13] better resembles reality in that aspect. During stance phase it uses a muscle-reflex model based upon the work of Geyer and Herr [16]. Furthermore, every model or simulation has simplifications, assumptions, or other aspects making it deviate from reality. This makes comparing simulations of the amputee gait with prosthesis, to the healthy gait data less insightful and less valid. Comparison with healthy gait data can only confirm if the prosthesis is capable of replicating healthy gait kinematics. It does not show that wearing the prosthesis will result in a more normal gait compared to other prostheses. There is a lack of a model that simulates the gait of a TF amputee wearing a commonly used knee prosthesis. Ideally, such a model uses a neurologically-based controller throughout the gait. This model could serve as baseline of comparison for newly developed and simulated prostheses. Having such a model also opens up exploring the possibilities of modifying the prosthetic leg for improving its functionality. An example of this is embedding a control moment gyroscope (CMG) in the prosthetic leg. Lemus *et al.* have

Nathan Timmers is with the Department of Biomechanical Engineering, Delft University of Technology, Delft 2628CD, The Netherlands.

already shown the potential of supporting the control of the posture with a CMG [17]. Using an CMG in the prosthetic leg can be used to increase the stride length or minimum toe clearance (MTC) [18]. Having more control over the prosthetic leg is especially helpful for preventing a trip. For fall prevention after a trip a quick and rapid long recovery step is sometimes needed. This requires sufficient extension movement, so that the prosthesis is fully extended at loading. Since TF amputees have little control over their prosthetic knee, this can be difficult to do with the prosthetic leg, as suggested by the result from Crenshaw *et al.* [8]. Even though some active prostheses have a form of fall prevention, for instance by switching to a reduced resistance mode, it does not always work well [7].

The main goal of this paper is to adjust the existing 3D neuromuscular model, such that it represents a TF amputee wearing a commonly used prosthesis. Then the gait is simulated, to evaluate its resemblance to a real amputee. The prosthesis selected to be used in the model, is the Otto Bock 3R60 knee. After an inquiry at a nearby rehabilitation center, it was found to be one of the most sold knee prosthesis in the Netherlands. The model is then used to explore the potential of fall prevention using a CMG located on the prosthetic leg. Thatte and Geyer [13] have simulated the gait of a TF amputee wearing their newly developed prosthesis. However, this model is in 2D and uses a torque generator during swing phase. The work of Song and Geyer [19] can be used to extend this. In their paper the gait of a healthy person is simulated in 3D using a muscle-reflex model throughout the whole gait. To develop a model of the 3R60 in Simulink, the thesis of Vandaele [20] was used. In his thesis he created a multi-body dynamic model of the 3R60.

The structure of this paper is as follows. First the methods used are explained in Section II. In Subsection II-A a general overview of the TF amputee model and of the model with the CMG added are given. In Subsection II-B the musculo-skeletal model is presented and in Subsection II-C the method of modeling the prosthesis is explained. Subsection II-D provides the neurological control method used to control the muscles. The methods for the exploratory study on fall prevention using a CMG are described in Subsection II-E. The optimization of the control gains is described in Subsection II-F. A brief description of how the data obtained from the simulation is processed is given in Subsection II-G. The approach for validating the model is presented in Subsection II-H Then the results on simulating the amputee gait, and the fall prevention are presented in Section III and discussed in Section IV. Finally the paper is concluded in Section V.

II. Methods

A. Model overview

The 3D TF amputee model is developed using Simulink [21] and is available via Github [22]. For the exploratory research on fall prevention, a CMG is added to the model which is controlled using a low- and high-level controller. An overview of how the model is build up can be found in Fig. 1. The amputee model consists of four main elements: the skeleton, prosthesis, muscles and neurological controller. Each separate element of the model is further explained in Subsection II-B to II-D. The fall prevention consists of three main elements: the CMG, the CMG controller, and the trip detector. The exact details of the model, controller, and obstacle are explained in Subsection II-E. The optimization method is described in Subsection II-F.

B. Musculo-skeletal model

The musculoskeletal model of Song and Geyer [19] is used as the starting point. From this model the right side is amputated, so the foot and shank of the amputated side are replaced with a prosthetic foot and shank. The amputated thigh is shortened to match a TF amputation of $11\,\mathrm{cm}$. The model resembles a human with a length of $1.8\,\mathrm{m}$ and a mass of approximately $77\,\mathrm{kg}$, including the prosthetic leg. The joints have soft joint limits in order to prevent violating anatomic joint limits. When a joint violates a joint limit, a stop torque τ_{st} is exerted on the joint to limit further joint limit violation. Song and Geyer use a soft knee joint limit if $5\,^\circ$ [19]. However, during normal gait this limit is exceeded every gait cycle. So the model relies on the extra torque provided by the soft knee joint limit. Therefore the soft knee joint limit was set to $1\,^\circ$, to reduce the model's reliance on this extra torque. Further details on joint limits, limb mass and inertia, limb length, and local axes definitions are given in Appendix A-1.

The vastii (VAS), the short head of biceps femoris (BFSH), the gastrocnemius (GAS), the soleus (SOL), and the tibialis anterior (TA) muscles are removed from the model on the amputated side. Due to the amputation the hamstrings (HAM) and rectus femoris (RF) muscles are no longer bi-articular and their length changes, as modeled in [13]. Studies have shown that muscle atrophy occurs in the hip muscles of TF amputees. This changes muscle properties such as muscle strength. The hip flexor muscles of the amputated leg are $25-40\,\%$ weaker compared to the intact leg. Similarly, the extensor muscles are $30-50\,\%$ weaker [23]–[25], the abductor muscles are up to $30\,\%$ weaker [26], and the adductor muscles are up to $70\,\%$ weaker [27]. The muscles are modeled using the muscle-tendon model of Geyer *et al.* [28] The details of the muscle-tendon model and the values of the muscle parameters are given in Appendix C-1.

C. Prosthesis model

The prosthetic leg consists of the 3R60 prosthetic knee, a shank, an ankle, and a foot. The prosthetic shank is a rod with a similar location of the center of mass (COM) as the intact shank. The prosthetic foot is connected to the prosthetic shank via the prosthetic ankle. This ankle is a simple revolute joint with high stiffness, resembling a rigid ankle. The exact mass and inertia of the prosthetic shank and foot are given in Appendix A-1. The 3R60 knee prosthesis, shown in Fig. 2(a) and Fig. 2(b), is developed by Otto Bock. The knee comprises of five axes and two hydraulic elements. The axes and hydraulic elements are linked together in such a way that the joint is poly-centric and has two degrees of freedom (DOFs). These two DOFs result in a different behavior for

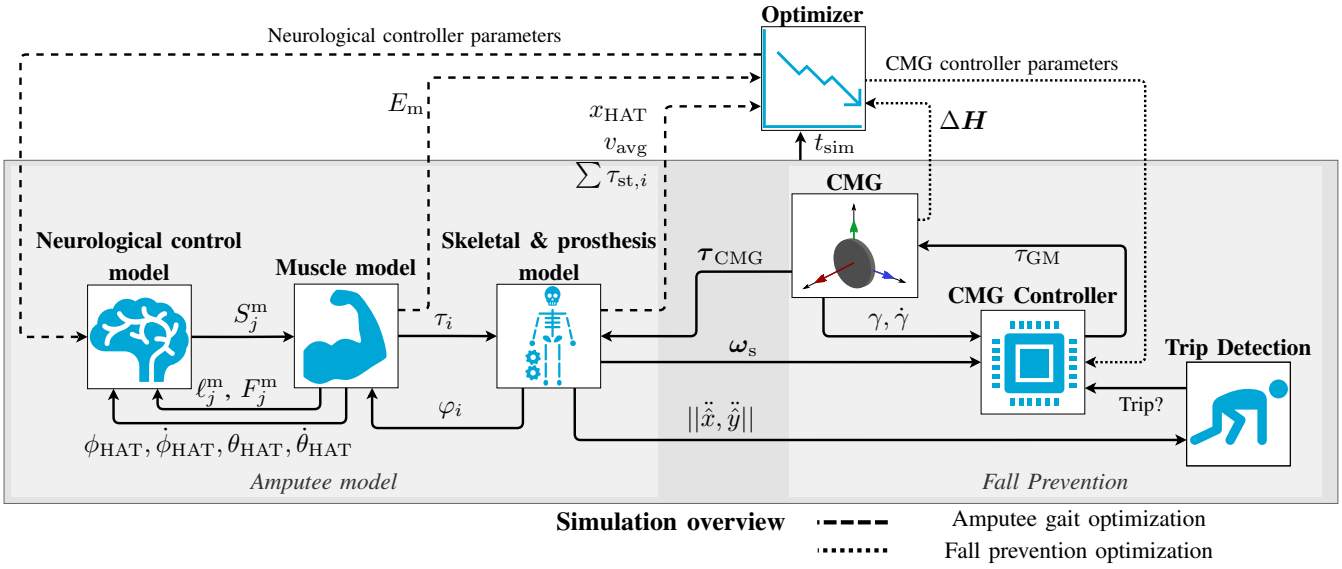

Fig. 1. Overview of the amputee model, which consist of the skeletal and prosthesis model, muscle model, and the neurological control model In the model the added control moment gyroscope (CMG) for the fall prevention case study is shown as well. The movement of the skeleton is determined by the joint torques τ_i, which is calculated from the muscle forces F_j^{m}. The muscle forces are calculated from the joint angles φ_i and muscle stimulations S_j^{m}. The muscle stimulations are controlled by the neurological controller, which calculates the required stimulations based on the trunk pitch angle and angular velocity $\phi_{\mathrm{HAT}}, \dot{\phi}_{\mathrm{HAT}}$, trunk roll angle and angular velocity $\theta_{\mathrm{HAT}}, \dot{\theta}_{\mathrm{HAT}}$, and muscle lengths ℓ_j^{m} and forces F_j^{m}. During gait optimizations only the neurological controller gains are optimized. The cost function uses the distance walked $\boldsymbol{x}_{\mathrm{HAT}}$, the average velocity v_{avg}, the sum of stop torques $\sum \tau_{\mathrm{st},i}$, the metabolic energy E_{m}, and the reached simulation time t_{sim}. For the fall prevention a CMG is added. During normal walking the angular velocity of the shank $\boldsymbol{\omega}_{\mathrm{s}}$ is canceled out by the controller to minimize the perturbation on the normal gait. The norm of the magnitude of the anterior-posterior and medio-lateral local shank acceleration $||\ddot{\hat{x}}, \ddot{\hat{y}}||$ is used for trip detection. If a trip occurs, a gimbal motor torque τ_{GM} is applied, resulting in a rotation of the gimbal motor and a gyroscopic moment of the CMG $\boldsymbol{\tau}_{\mathrm{CMG}}$ so that a fall is prevented. During fall prevention optimization the CMG controller gains are optimized such that the exchanged angular momentum $\Delta \boldsymbol{H}$ is minimized.

stance and swing phase. One hydraulic element is only used during stance phase flexion. The other hydraulic element is mainly used during swing phase flexion. The elements have different stiffness and damping characteristics. Vandaele created a multi-body model of the 3R60 knee in his thesis [20]. This model was used to develop a model of the 3R60 knee in Simulink. Details on the properties of the 3R60 are presented in Appendix B. Furthermore, a comparison between the Simulink model and the model of Vandaele is shown here as well.

(a) Front side. (b) Back side.

Fig. 2. 3R60 knee by Otto-bock. Images taken from the Otto Bock image library [29].

D. Neurological control model

The neurological control model of Song and Geyer [19] is used to control the muscles. The control model consists of ten different reflex modules that entail a certain functionality of the gait. Examples of such functionalities are realizing a compliant leg at landing, and preventing knee hyper-extension during stance. In the muscle-reflex model robust foot placement is incorporated using a target leg angle (TLA) principle based on the work of Yin *et al.* [30]. For the robust foot placement the intact leg makes use of the RF muscle length to calculate the leg clearance, which is needed for the algorithm. However, in the amputated leg this muscle is no longer bi-articular and cannot provide the leg clearance information. Instead, the leg length is calculated via the relative position of ankle with respect to the hip. This is similar to what was done in [13]. Since the amputee model is not symmetric it will have a tendency to walk in a large circular motion. To counteract this motion the lateral position and the integrated lateral position are fed back to the TLA calculator. This influences the lateral control such that the model will tend towards the lateral zero position. The muscle-reflex model is similar for the intact and prosthetic leg for the muscles present in both legs. However, the gains, offsets, and other control parameters have different values. This represents the fact that the legs are dissimilar. The values of the control parameters are obtained through optimization.

E. Fall prevention using a control moment gyroscope

For the exploratory research on fall prevention after a trip using a CMG, an obstacle was placed such that the intact leg was tripped in late swing while walking $1.2\,\mathrm{m/s}$. For preventing a fall after a trip in late swing a lowering strategy is most often used [31]. A lowering strategy consists of bringing the tripped foot quickly to the ground, then the contra-lateral

limb takes a recovery step [32], [33]. Taking this recovery step with the prosthetic leg can be difficult, due to limited control of the knee. Hence the potential benefits of using a CMG for preventing a fall can be shown.

An accelerometer was placed on the COM of the intact shank for trip detection. The acceleration is sampled at 1000 Hz and then filtered with a highpass and lowpass filter with a cutoff frequency of 3 Hz and 80 Hz, similar as was done in [34]. The magnitude of acceleration in the $\hat{\boldsymbol{x}}$ and $\hat{\boldsymbol{y}}$ direction of the local shank coordinate frame was fed into a simple detection algorithm. It detects if the value goes above a certain threshold. If this is true, then it classifies the data as a trip. Furthermore, a sensor was added to measure the angular velocity of the COM of the prosthetic shank. This sensor is also sampled at 1000 Hz. The CMG added to the model is embedded in the prosthetic shank. Fig. 3 shows the local coordinate frames of the CMG and its attachment point to the shank. If the gimbal axis angle γ equals zero the axes of the local CMG coordinate frame are parallel with the axes of the local shank coordinate frame: $\hat{\boldsymbol{x}}||\hat{\boldsymbol{g}}_s$, $\hat{\boldsymbol{y}}||\hat{\boldsymbol{g}}_t$, $\hat{\boldsymbol{z}}||\hat{\boldsymbol{g}}_g$. When the CMG has an angular momentum $\boldsymbol{H}$, then an angular velocity of the gimbal axis $\dot{\boldsymbol{\gamma}}$, or of the shank $\boldsymbol{\omega}_\mathrm{s}$ result in a gyroscopic torque $\boldsymbol{\tau}_\mathrm{CMG}$ being generated by the CMG. This gyroscopic torque and the gimbal motor torque result in a reaction torque being exerted on the shank $\boldsymbol{\tau}_\mathrm{s}$. This torque can be split up in an anterior-posterior τ_AP, a medio-lateral τ_ML, and a longitudal τ_L component:

$$\begin{aligned}\boldsymbol{\tau}_\mathrm{s}(t) &= -\boldsymbol{\tau}_\mathrm{CMG}(t) = -\dot{\boldsymbol{H}}(t)\\ &= -(\dot{\boldsymbol{\gamma}}(t) + \boldsymbol{\omega}_\mathrm{s}(t)) \times \boldsymbol{H}(t) - \boldsymbol{\tau}_\mathrm{GM}(t)\\ &= \tau_\mathrm{ML}(t)\hat{\boldsymbol{x}} + \tau_\mathrm{AP}(t)\hat{\boldsymbol{y}} + \tau_\mathrm{L}(t)\hat{\boldsymbol{z}}.\end{aligned} \tag{1}$$

A more detailed version of the calculation is shown in Appendix D-2.

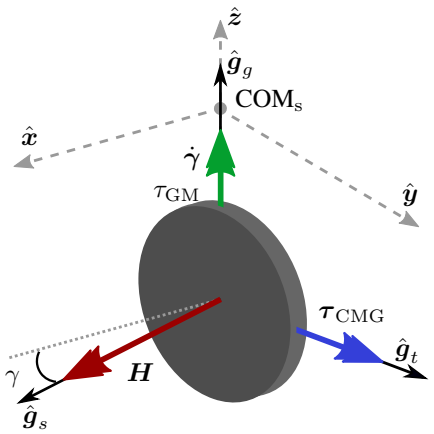

Fig. 3. Model of the control moment gyroscope (CMG), with its local coordinate frame with unit direction vectors $(\hat{\boldsymbol{g}}_s, \hat{\boldsymbol{g}}_t, \hat{\boldsymbol{g}}_g)$. The CMG is attached below the center of mass of the shank $\mathrm{COM_s}$. The shank has a local coordinate frame with unit direction vectors $(\hat{\boldsymbol{x}}, \hat{\boldsymbol{y}}, \hat{\boldsymbol{z}})$. When $\gamma = 0$, $\hat{\boldsymbol{g}}_s$ aligns with $\hat{\boldsymbol{x}}$. The flywheel of the CMG rotates with a velocity Ω around the $\hat{\boldsymbol{g}}_s$ axis. The gimbal motor actuates the $\hat{\boldsymbol{g}}_g$ axis resulting in an angle γ, and an angular velocity $\dot{\boldsymbol{\gamma}} = \dot{\gamma}\hat{\boldsymbol{g}}_g$. The CMG has angular momentum $\boldsymbol{H} = H\hat{\boldsymbol{g}}_s$. The magnitude of the angular momentum $H = I_\mathrm{ss}\Omega$, where I_ss is the inertia of the CMG around the $\hat{\boldsymbol{g}}_s$ axis. The shank has an angular velocity $\boldsymbol{\omega}_\mathrm{s} = (\omega_{\hat{\boldsymbol{x}}}, \omega_{\hat{\boldsymbol{y}}}, \omega_{\hat{\boldsymbol{z}}})$. Movement of the gimbal motor and the shank results in a gyroscopic moment $\boldsymbol{\tau}_\mathrm{CMG}$, which yields a reaction torque on the shank $\boldsymbol{\tau}_\mathrm{s} = -\boldsymbol{\tau}_\mathrm{CMG}$.

The properties of the CMG are based on the research of Jabeen *et al.* [18]. The angular impulse exerted in this study was achieved using a CMG with a diameter of 80 mm, a mass of 1 kg of which 50 % is located at the rim, and a flywheel angular velocity of $\Omega = 2100\,\mathrm{rad/s} \approx 20\,\mathrm{krpm}$. The inertia of the flywheel I_ss around the $\hat{\boldsymbol{g}}_s$ axis and the other moments of inertia are calculated from these properties. This is further explained in Appendix D-1. The maximum torque that can be exerted by the gimbal motor (GM) τ_lim is set to 15 Nm, which was deemed to be a realistic limit for this size of CMG. The muscle-reflex parameters for the amputee gait were reoptimized with the CMG inactive, so that the model could adapt to the extra mass and inertia of the CMG.

When the CMG is active, then the torque exerted by the gimbal motor is controlled via a feed-forward term and two high-level controllers. The total gimbal motor torque is:

$$\begin{aligned}\tau_\mathrm{GM}(t) = I_\mathrm{ss}\Omega(\omega_{\hat{\boldsymbol{y}}}\cos(\gamma(t)) - \omega_{\hat{\boldsymbol{x}}}(t)\sin(\gamma(t)))\\ + \begin{cases}\tau_\mathrm{w}(t), & \text{if walking}\\ \tau_\mathrm{f}(t), & \text{if trip.}\end{cases}\end{aligned} \tag{2}$$

The 'walk controller' applies a torque τ_w to ensure minimal perturbation of the gait. This is achieved by canceling out the angular velocity of the shank, hence minimizing parasitic moments. The torque of the 'fall prevention controller' τ_f is calculated based on an algorithm similar to the robust foot placement algorithm from Yin *et al.* [30]. This algorithm contains gains which need to be optimized. For this the same method as for the optimization of the neurological control gains. The details of the controllers are given in Appendix D-2.

F. Optimization

The muscle-reflex model consists of gains, offsets, and other parameters. These parameters are different for the intact and prosthetic leg, and are obtained through optimization. Initial joint angles, initial velocity of the model, muscle stimulation levels are optimized as well. In total there are 163 parameters which are optimized when optimizing the amputee gait. The CMG fall prevention controller gains are optimized during a different optimization. In that case the muscle-reflex parameters are kept constant and only the seven fall prevention controller gains are used as optimization variables. During optimization the model is simulated and the cost function is evaluated using the data from the simulation. The simulation data is sampled at 30 Hz, except for the fall prevention optimization. In that case the data is sampled at 1000 Hz. For both optimizations, the optimization algorithm used is the covariance matrix adaption evolution strategy (CMAES) algorithm from [35], similar to what was done in [13], [19]. The cost function J used for the optimization is defined as

$$\begin{aligned}J = \alpha \cdot \underbrace{\frac{E_\mathrm{m}}{m \cdot ||\Delta x_\mathrm{COM}, \Delta y_\mathrm{COM}||}}_{\mathrm{CoT}} + \beta \cdot \underbrace{|v_\mathrm{avg} - v_\mathrm{ref}|}_{\mathrm{TVC}}\\ + \gamma \cdot \underbrace{\sum \tau_\mathrm{st}}_{\mathrm{STC}} + \delta \cdot \underbrace{\frac{T_\mathrm{sim}}{t_\mathrm{end}} - 1}_{J_t} + \epsilon \cdot \underbrace{||\Delta \boldsymbol{H}(t)||_\mathrm{max}}_{J_{\Delta \boldsymbol{H}}}.\end{aligned} \tag{3}$$

It consists of five elements: the CoT, target velocity cost (TVC), the stop torque cost (STC), the time cost J_t, and the cost of maximum exchanged angular momentum $J_{\Delta \boldsymbol{H}}$. The time cost was added to ensure higher costs for simulations that do not reach the set end time T_{sim}, but stop at time t_{end}, both in seconds. The cost of transport (CoT) gives a measure of how energy efficient the gait is by dividing the metabolic energy E_{m} with the mass and the distance walked. This gives a trade-off between the energy spent and the distance reached. The metabolic energy of the muscles is calculated using the updated muscle expenditure model of Umberger [36]. Details of this model are further explained in Appendix C-2. The target velocity cost (TVC) is used to let the average velocity of the model v_{avg} converge to a desired reference velocity v_{ref} in $\mathrm{m/s}$. The average velocity of the model is defined as mean of the norm of the velocity in anterior x and lateral y direction. This is useful for comparing the results with literature and to compare the differences of the simulated gait at different velocities. The stop torque cost (STC) is the sum of all the joint stop torques τ_{st}. The cost for the maximum exchanged angular momentum is only used when optimizing the CMG controller for fall prevention. The cost minimizes the maximum exchanged angular momentum $||\Delta \boldsymbol{H}(t)||_{\mathrm{max}}$. During optimization of the amputee gait this cost is not used. Every element of the cost function is multiplied with a cost factor. This puts more emphasis on a certain elements and less emphasis on other elements of the cost function. The cost factors for both the amputee gait and fall prevention optimization are given in Table I.

In the amputee gait optimization, the model walks over four different terrains, one of which is a flat terrain. The other terrains have small height changes that represent a rough terrain. The first $10\,\mathrm{m}$ of the rough terrain are still flat so that it does not impact the transient response of the model. After $10\,\mathrm{m}$, the height is changed randomly every meter. After creating the rough terrain, the height changes are scaled such that the maximum height change is $1\,\mathrm{cm}$. An example of a generated rough terrain is shown in Fig. E-1.

To ensure a realistic gait a self-collision detector was added. This detects whether the leg segments collide with each other and ends the simulation if that is the case. The algorithm calculates the distance between two leg segments by using the method of calculating the distance between skew lines. The algorithm is described in Appendix E-1.

TABLE I
VALUES OF THE OPTIMIZATION COST FACTORS FOR BOTH THE AMPUTEE GAIT AND THE FALL PREVENTION OPTIMIZATION.

	α $(\mathrm{s^2/m})$	β $(\mathrm{s/m})$	γ $(\mathrm{s^2 kg^{-1} m^{-2}})$	δ $(-)$	ϵ $(\mathrm{kg^{-1} m^{-2} s^{-3}})$
Amputee gait	1	100	0.01	1e5	0
Fall prevention	1	100	0.01	1e5	15

G. Data processing

For final evaluation of the gait, the models are simulated walking on a flat ground for $30\,\mathrm{s}$. The simulation data is then processed and compared. The data acquired from the model for evaluation is sampled at $1000\,\mathrm{Hz}$. During post-processing the data is divided into sections corresponding to a stride. Then the data is linearly interpolated such that each section has data points with $0.5\,\%$ increments for $0-100\,\%$. Then the data is averaged and the standard deviation is calculated per leg. The first four steps are not taken into account.

H. Model validation

The performance of the amputee model is evaluated to see if the model represents a real amputee. Several parameters of the simulated gait of the amputee and healthy model are compared. For comparing the simulations of the healthy and amputee model the stance time t_{St}, swing time t_{Sw}, double stance time t_{DS}, step time t_{s}, step length ℓ_{s}, maximum ankle power during stance $P_{\mathrm{a,max}}$, mean anterior-posterior braking and propelling ground impulses $p_{\mathrm{x_b}}$, $p_{\mathrm{y_p}}$, and mean vertical ground impulse p_{z} are compared. These measures have been compared between healthy and TF amputees in literature using experimental data [4], [37]–[44]. These studies can be used to compare the differences found in literature to the differences found in the simulated amputee and healthy gait. The step length, and time are defined as described in [45]. For the double stance time the result for IP means the double stance time for when the model steps from the intact leg onto the prosthetic leg. For each parameter, the mean, standard deviation, and the average and standard deviation of the absolute symmetry index (ASI) are given. The mean is calculated by averaging the parameter over all the strides. The ASI of the healthy model is defined as the difference between the left (L) and right (R) leg gait parameter value:

$$\mathrm{ASI} = \frac{\mathrm{L}-\mathrm{R}}{0.5(\mathrm{L}+\mathrm{R})} \cdot 100\,\%. \tag{4}$$

The variables L and R correspond to a parameter value calculated for a certain stride. Positive values of the ASI mean that the parameter value of the left side is larger than the right side. The average ASI is calculated by averaging over the ASI values for each stride. For the amputee model the left leg is the intact leg, and the right is the prosthetic leg. The parameters for the gait simulations where the model has an inactive and active CMG embedded, are compared as well. This comparison shows how much an active CMG perturbs the normal gait.

The simulated healthy model is similar to the model of Song and Geyer [19]. Only the soft joint limit and muscle expenditure model have been changed and the muscle-reflex parameters have been reoptimzed. The simulated healthy gait is compared to experimental data of healthy gait from Fukuchi *et al.* [46] by calculating the correlation between the simulated and experimental gait data. The correlation is calculated for the joint angles, joint torques, and the ground reaction forces (GRF), as was done by Song and Geyer [19].

III. RESULTS

A. Gait simulation

Fig. 4(a) and Fig. 5(a) show the average joint angles obtained from the data of healthy humans walking at $0.9\,\mathrm{m/s}$ and

$1.2\,\mathrm{m/s}$ from Fukuchi [46], and from the simulated healthy model walking with the same velocity. For the simulation data the standard deviation is also shown in the figures. The figures include the correlation values of the data from Fukuchi and the simulation. In Fig. 4(b) and Fig. 5(b) the average and standard deviation of the joint angles are shown, which are obtained from the simulation of an amputee walking at $0.9\,\mathrm{m/s}$ and $1.2\,\mathrm{m/s}$. Fig. 5(c) and Fig. 5(d) show the average and standard deviation of the joint angles obtained from the simulation of an amputee walking at $1.2\,\mathrm{m/s}$ with an inactive and active CMG.

In Table II the average and standard deviation of the stance time, swing time, double stance time, step time, and step length are presented for both legs. Similarly, in Table III presents the average and standard deviation of the maximum ankle power during stance, mean anterior-posterior braking and propelling ground impulse, and mean vertical ground impulse for both legs. For all parameters the average and standard deviation of the ASI are given as well. The data of healthy gait simulations is averaged over both legs.

In Appendix F-1 extra figures of the gait simulations are give. Fig. F-1 to Fig. F-8 show the average and standard deviation of the joint torques, joint powers, GRF, and muscle activation levels for simulations of both the healthy and amputee model walking at both speeds. The figures for the model walking at $1.2\,\mathrm{m/s}$ show data for the amputee walking with inactive and active CMG as well. Data files of the results and videos of the different simulations are available via Github [22].

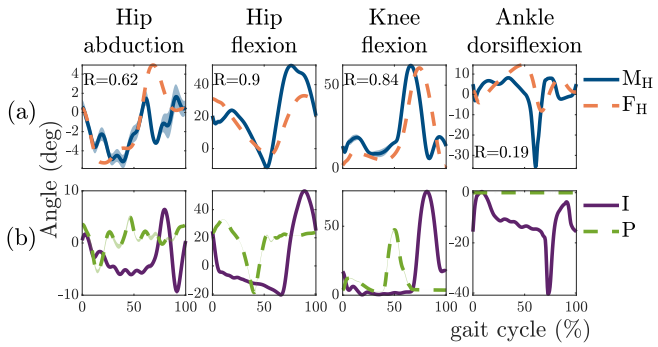

Fig. 4. Average joint angles and standard deviation during a stride of (a) a healthy model (M_H) compared to data from Fukuchi (F_H) [46] and (b) for the intact (I) and prosthetic (P) leg of the amputee model walking on a flat ground with $0.9\,\mathrm{m/s}$.

B. Fall prevention using a control moment gyroscope

In Fig. 6 the CMG angle, angular velocity, torque, and the exchanged angular momentum are shown. The data is averaged over a stride for when the model is just walking and presented in Fig. 6(a). In Fig. 6(b) the response of the CMG fall prevention controller is shown for a successful fall prevention after a trip. The moment of collision with the obstacle is around $t = 7.2\,\mathrm{s}$. The time during which the fall prevention controller is active is between $t = 7.4\,\mathrm{s}$ and $t = 7.9\,\mathrm{s}$. Both are indicated in the figures as well. In Appendix F-2 one extra figure on fall prevention is given. Fig. F-9 shows the GRF around the moment of collision and fall prevention. Data files of the results and videos of the simulations are available via Github [22].

TABLE II

THE AVERAGE AND STANDARD DEVIATION OF THE STANCE TIME t_{St}, SWING TIME t_{Sw}, DOUBLE STANCE TIME t_{DS}, STEP TIME t_{s}, STEP LENGTH ℓ_{s} OBTAINED FROM THE SIMULATIONS OF THE HEALTHY AND AMPUTEE MODEL. THE AVERAGE AND STANDARD DEVIATION OF THE ABSOLUTE SYMMETRY INDEX (ASI) IS GIVEN FOR THE PARAMETERS AS WELL. FOR THE AMPUTEE MODEL THE RESULTS ARE GIVEN FOR THE INTACT SIDE (I) AND PROSTHETIC SIDE (P) WITHOUT CONTROL MOMENT GYROSCOPE (CMG), FOR THE INTACT ($\mathrm{I_{CI}}$) AND PROSTHETIC ($\mathrm{P_{CI}}$) LEG WITH INACTIVE CMG, AND FOR THE THE INTACT ($\mathrm{I_{CA}}$) AND PROSTHETIC ($\mathrm{P_{CA}}$) LEG WITH ACTIVE CMG. THE DATA GIVEN OF THE HEALTHY MODEL ($\mathrm{M_H}$) IS AVERAGED OVER BOTH SIDE.

		$0.9\,\mathrm{m/s}$		$1.2\,\mathrm{m/s}$	
		Mean	ASI	Mean	ASI
t_{St} (s)	$\mathrm{M_H}$	0.70 (0.01)	0.21 (1.32)	0.65 (0.00)	-0.11 (0.74)
	I	0.94 (0.01)	49.40 (0.74)	0.69 (0.01)	28.86 (0.68)
	P	0.57 (0.00)		0.52 (0.00)	
	$\mathrm{I_{CI}}$			0.67 (0.08)	8.91 (9.77)
	$\mathrm{P_{CI}}$			0.61 (0.02)	
	$\mathrm{I_{CA}}$			0.70 (0.09)	12.82 (11.20)
	$\mathrm{P_{CA}}$			0.61 (0.02)	
t_{Sw} (s)	$\mathrm{M_H}$	0.50 (0.00)	-0.02 (1.47)	0.47 (0.00)	0.14 (0.68)
	I	0.37 (0.00)	-66.36 (1.21)	0.38 (0.00)	-37.81 (0.84)
	P	0.75 (0.01)		0.55 (0.01)	
	$\mathrm{I_{CI}}$			0.45 (0.01)	-11.92 (13.16)
	$\mathrm{P_{CI}}$			0.51 (0.06)	
	$\mathrm{I_{CA}}$			0.45 (0.01)	-16.68 (11.99)
	$\mathrm{P_{CA}}$			0.53 (0.07)	
t_{DS} (s)	$\mathrm{M_H}$	0.10 (0.00)	-0.30 (1.90)	0.09 (0.00)	0.06 (1.78)
	IP	0.09 (0.00)	-18.79 (1.65)	0.08 (0.00)	27.16 (3.68)
	PI	0.10 (0.00)		0.06 (0.00)	
	$\mathrm{I_{CI}P_{CI}}$			0.09 (0.01)	21.40 (13.16)
	$\mathrm{P_{CI}I_{CA}}$			0.07 (0.01)	
	$\mathrm{I_{CA}P_{CI}}$			0.10 (0.02)	32.89 (15.18)
	$\mathrm{P_{CA}I_{CA}}$			0.07 (0.01)	
t_{s} (s)	$\mathrm{M_H}$	0.61 (0.01)	-0.18 (1.04)	0.56 (0.00)	0.14 (0.38)
	I	0.46 (0.00)	-59.01 (1.32)	0.46 (0.00)	-28.97 (0.99)
	P	0.85 (0.01)		0.61 (0.01)	
	$\mathrm{I_{CI}}$			0.54 (0.01)	-7.27 (10.30)
	$\mathrm{P_{CI}}$			0.58 (0.07)	
	$\mathrm{I_{CA}}$			0.54 (0.02)	-10.04 (11.80)
	$\mathrm{P_{CA}}$			0.60 (0.08)	
ℓ_{s} (m)	$\mathrm{M_H}$	0.55 (0.02)	0.54 (2.96)	0.68 (0.01)	-0.32 (1.73)
	I	0.42 (0.00)	-53.66 (1.24)	0.59 (0.01)	-20.92 (1.76)
	P	0.73 (0.00)		0.72 (0.00)	
	$\mathrm{I_{CI}}$			0.68 (0.12)	-6.41 (5.78)
	$\mathrm{P_{CI}}$			0.71 (0.03)	
	$\mathrm{I_{CA}}$			0.67 (0.13)	-3.11 (13.57)
	$\mathrm{P_{CA}}$			0.68 (0.04)	

IV. Discussion

A. Gait simulation

This paper proposed an adjustment to an existing 3D neuromuscular model, such that it represents a TF amputee wearing the Otto Bock 3R60 knee prosthesis. The simulated amputee gait at $0.9\,\mathrm{m/s}$ and $1.2\,\mathrm{m/s}$ resembles the gait of a TF amputee in multiple aspects. It shows asymmetric characteristics, also contra-lateral vaulting can be seen which is common in TF amputees as well. The vaulting characteristic is also visible through the maximum ankle power during single stance [47]. This value is greater for the intact ankle of a TF amputee than for an ankle in healthy humans. The simulated gait shows this characteristic for both velocities. The other gait parameters of

TABLE III

THE AVERAGE AND STANDARD DEVIATION OF THE MAXIMUM ANKLE POWER DURING STANCE $P_{a,max}$, MEAN ANTERIOR-POSTERIOR BRAKING AND PROPELLING GROUND IMPULSES p_{x_b}, p_{y_p}, AND MEAN VERTICAL GROUND IMPULSE p_z OBTAINED FROM THE SIMULATIONS OF THE HEALTHY AND AMPUTEE MODEL. THE AVERAGE AND STANDARD DEVIATION OF THE ABSOLUTE SYMMETRY INDEX (ASI) IS GIVEN FOR THE PARAMETERS AS WELL. FOR THE AMPUTEE MODEL THE RESULTS ARE GIVEN FOR THE INTACT SIDE (I) AND PROSTHETIC SIDE (P) WITHOUT CONTROL MOMENT GYROSCOPE (CMG), FOR THE INTACT (I_{CI}) AND PROSTHETIC (P_{CI}) LEG WITH INACTIVE CMG, AND FOR THE THE INTACT (I_{CA}) AND PROSTHETIC (P_{CA}) LEG WITH ACTIVE CMG. THE DATA GIVEN OF THE HEALTHY MODEL (M_H) IS AVERAGED OVER BOTH SIDE.

		0.9 m/s		1.2 m/s	
		Mean	ASI	Mean	ASI
$P_{a,max}$ (W/kg)	M_H	1.16 (0.08)	-1.27 (7.93)	1.06 (0.02)	0.33 (1.42)
	I	2.08 (0.07)	-	2.91 (0.06)	-
	I_{CI}			2.86 (0.51)	-
	I_{CA}			2.70 (0.60)	-
p_{x_b} (Ns/kg)	M_H	-0.21 (0.02)	2.22 (10.39)	-0.27 (0.02)	-1.06 (6.81)
	I	-0.39 (0.01)	13.28 (1.89)	-0.47 (0.01)	101.92 (4.96)
	P	-0.34 (0.01)		-0.15 (0.01)	
	I_{CI}			-0.30 (0.06)	31.82 (21.66)
	P_{CI}			-0.22 (0.05)	
	I_{CA}			-0.34 (0.06)	54.93 (36.27)
	P_{CA}			-0.20 (0.06)	
p_{x_p} (Ns/kg)	M_H	0.21 (0.01)	-1.91 (7.16)	0.28 (0.01)	0.40 (4.63)
	I	0.68 (0.01)	151.79 (1.06)	0.45 (0.01)	73.17 (3.89)
	P	0.09 (0.00)		0.21 (0.01)	
	I_{CI}			0.42 (0.03)	72.69 (13.12)
	P_{CI}			0.20 (0.02)	
	I_{CA}			0.40 (0.05)	71.76 (11.83)
	P_{CA}			0.19 (0.03)	
p_z (Ns/kg)	M_H	5.93 (0.05)	0.16 (1.04)	5.50 (0.04)	-0.10 (1.04)
	I	8.10 (0.07)	51.58 (0.84)	6.23 (0.05)	37.42 (0.98)
	P	4.78 (0.03)		4.27 (0.04)	
	I_{CI}			5.93 (0.69)	15.51 (9.36)
	P_{CI}			5.04 (0.10)	
	I_{CA}			6.19 (0.77)	19.42 (12.08)
	P_{CA}			5.06 (0.12)	

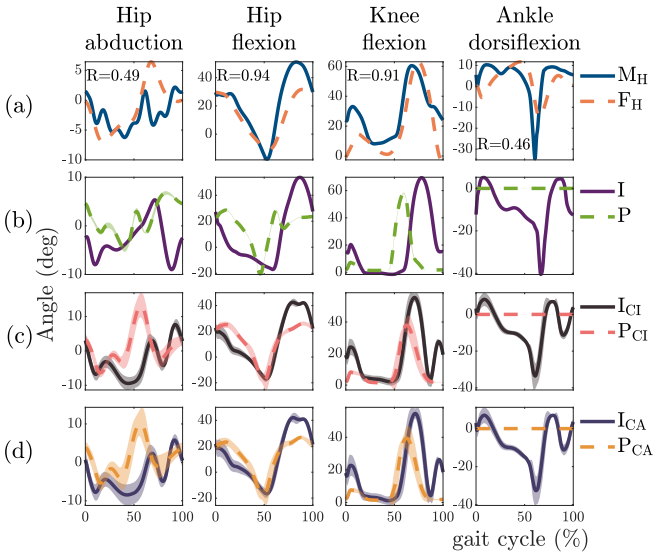

Fig. 5. Average joint angles and standard deviation during a stride of (a) a healthy model (M_H) compared to data from Fukuchi (F_H) [46], and (b) for the intact (I) and prosthetic (P) leg, and (c) for the intact (I_{CI}) and prosthetic (P_{CI}) with inactive CMG, and (d) for the intact (I_{CA}) and prosthetic (P_{CA}) leg with active CMG of the amputee model walking on a flat ground with $1.2\,\mathrm{m/s}$.

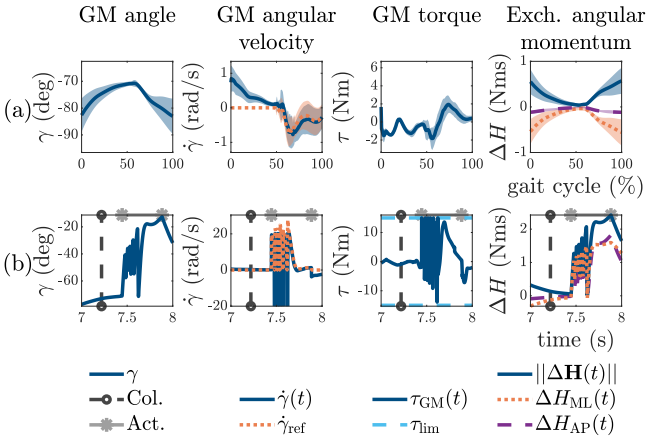

Fig. 6. Amputee model walking with CMG at $1.2\,\mathrm{m/s}$ with (a) the average data for the control moment gyroscope during a stride, and (b) the control response for successful fall prevention. The moment of collision (Col.) with the obstacle is around $t = 7.2\,\mathrm{s}$. The time the fall prevention response is active (Act.) are indicated in the fall prevention plots, which is between $t = 7.4\,\mathrm{s}$ and $t = 7.9\,\mathrm{s}$.

the simulated amputee gait for $1.2\,\mathrm{m/s}$ show similar positive or negative asymmetry as expected from literature [42], [44]. For example, the stance time is longer for the intact leg, and the swing and step time are longer for the prosthetic leg. Also, the step length of the prosthetic leg is larger. Although, in general the magnitude of the ASI is larger than found in [42], [44]. For the simulated gait walking at $0.9\,\mathrm{m/s}$ there are several deviations from literature. The model has a longer double stance time when stepping from the prosthetic leg onto the intact leg. Experiments have shown that the opposite is true [42], [44]. Furthermore, for the prosthetic leg the mean anterior-posterior propelling impulse is smaller than the braking impulse, which should be larger according to Schaarschmidt *et al.* [44]. For the intact leg this should be the opposite to the prosthetic leg, but this is also not the case. The other gait parameters do agree with literature with regards to positive or negative asymmetry. The change in asymmetry values between the different velocities also differs from what was found in [42], [44]. The change in asymmetry for the swing time is about two times bigger than found in [42]. For the stance, and step time, the change in asymmetry is much larger than found in literature [42], [44]. Furthermore, the mean impulse asymmetries of the simulation are dissimilar across different velocities, but they should be similar [42], [44].

The simulated healthy gait resembles human movement as well. The healthy gait at $1.2\,\mathrm{m/s}$ has similar values for the joint angle and GRF correlation factor as achieved by Song and Geyer [19]. However, the joint torque correlation is worse. For the healthy gait at $0.9\,\mathrm{m/s}$ all correlation factors are worse, except for the hip abduction angle correlation. The difference in joint torque correlation is interesting, because the joint angle correlation is quite similar. Changes in the soft joint limit and muscle expenditure might be the cause for this. These were the main differences between the healthy model of Song and Geyer and of this paper. These changes led to different joint torques, but not too dissimilar joint angles. In general the ankle angle correlation is low. The ankle is modeled as a 1 DOF

revolute joint, which in reality is not the case. This may be the source for the low correlation.

The simulated gait for both the amputee and healthy model walking at $0.9\,\mathrm{m/s}$ deviates more from literature. Simplifications in the control model might be the reason for this. It seems that especially in the coronal plane the model has difficulties in maintaining balance at lower velocities. Oscillatory hip abduction torque during walking supports this hypothesis. The lateral neurological control is only dependent on the target leg angle principle. This may be an algorithm which is too coarse and not detailed enough, resulting in oscillations. Furthermore, the magnitude of the ASI and the change in ASI between different velocities is often larger than found by Schaarschmidt *et al.* and Nolan *et al.* [42], [44]. Apart from modeling assumptions and simplifications, there is the human factor which is not present in the model. For instance, results from Schaarschmidt *et al.* suggest that amputees are cautious when stepping onto the prosthetic leg [44]. The model has no fear factor and is not cautious. The optimization finds a set of control gains, which result in successful and relatively optimal gait. The missing human factor contributes to the fact that the model deviates from reality.

The response of the 3R60 prosthetic knee during the simulated gait shows similar characteristics to experimental findings by Blumentritt *et al.* [48]. However, the maximum swing-phase flexion for both velocities, and the maximum stance phase flexion for $0.9\,\mathrm{m/s}$, is lower. Still, it does show typical characteristics of the 3R60 during walking. So the 3R60 model is deemed sufficiently accurate for simulating the gait of a TF amputee wearing a 3R60.

It was found that the amputee model is numerically sensitive. Difficulty with lateral control could be one of the reasons. This can cause small numerical deviations to be enlarged, yielding a different result. This problem was mainly seen when comparing gait simulations on rough terrain on different computers, or when the model was changed. To overcome this, the gait parameters can be reoptimized, which gives a feasible gait again. On flat terrain the simulation produces more reproducible results. The gait is similar and successful on both computers. Setting the solver step time to fixed, instead of variable, might give a more reproducible simulation on rough terrain. However, the simulation time will most likely increase due to this changed setting.

The benefits of having a model of a TF amputee wearing a common knee prosthesis could immediately be put into practice with the case study. The gait parameters, and joint angles for the amputee gait with inactive or active CMG walking at $1.2\,\mathrm{m/s}$ differ only slightly between each other. Entirely canceling out the gyroscopic torque is not feasible, so this small difference is a sufficiently good performance of the walk controller. Adding the CMG introduces a slight deviation from literature with respect to the gait parameters. The braking impulse of the intact leg is smaller than its propulsive impulse, and for the prosthetic leg the propulsive impulse is smaller than its braking impulse. This was not the case for the amputee gait without CMG walking at $1.2\,\mathrm{m/s}$. Another interesting observation, is that the amputee gait with both inactive and active CMG is more symmetric compared to the amputee gait without CMG. For the gait with inactive CMG all the gait parameters have an ASI value closer to zero than for the amputee gait without CMG. The gait parameters for the simulation with active CMG shows a similar trend. The exception is the double stance time, which is more asymmetric than the amputee gait without CMG. One of the explanations for the decreased asymmetry is that the inertial characteristics of the prosthetic leg with CMG resemble the intact leg more closely. One way to show this is via the natural frequency of the shank-foot combination. The natural frequency of the healthy shank-foot combination is $5.22\,\mathrm{rad/s}$, of the prosthetic shank-foot combination is $4.74\,\mathrm{rad/s}$, and of the prosthetic shank-foot with CMG combination is $5.27\,\mathrm{rad/s}$. Details of the calculation can be found in Appendix D-1. Several studies have found results that suggest that increasing the inertial load will result in a more normal gait pattern [49]–[51]. However, one of the studies found almost no impact on the gait [52], and another even some negative impact [53]. These different conclusions show that there is not yet a uniform conclusion, but it remains an interesting topic for research.

Another added benefit of the work of this study, is that the 3D healthy model can now also be used for further research, since the model made available by Song and Geyer still contained old Simulink blocks, which could not be used for efficient optimization.

B. Fall prevention using a control moment gyroscope

In the case study a fall was prevented after letting the model trip over an obstacle. The data of the applied GM torque shows oscillations. This is because the prosthetic leg bounces on the ground several times during the fall prevention. In Fig. F-9 the spikes in anterior-posterior and vertical GRF from the bouncing onto the ground are visible. Both the fall prevention of the model and the controller do not provide sufficient leg clearance.

The moment of tripping had to be carefully selected, otherwise no successful fall prevention could be achieved. One of the reasons for this behavior is the current foot-placement algorithm, which cannot execute a multi-step perturbation recovery. Furthermore, the neurological control gains are optimized for walking and not for preventing a fall. This is one of the reasons why the fall prevention strategy of the model is not effective, resulting in not enough ground clearance. Finally, the fall prevention simulation was found to be even more numerically sensitive than the amputee gait simulations. Tiny differences in the model, especially when related to integrator blocks, resulted in a failed fall prevention. Due to these limitations and deficiencies, no conclusion can be made with regards to the potential of using a CMG for fall prevention.

C. Future research

For further development of amputee simulation with a 3R60, it is necessary to do experiments. To the knowledge of the author there is currently no data available of amputees walking with a 3R60. This data would be useful for validating the

simulation and having a benchmark to aim for. Also, more research should be conducted on the neurological control model, especially the lateral control. A velocity of around $1.2\,\mathrm{m/s}$ is generally considered to be a fast gait for TF amputees [4], [37], [54]. So the focus should be on simulating slower gaits more realistically. This will increase the usefulness of the model. Investigating alternatives for the muscular model may also provide a solution for simulating slower gaits. Currently, the coronal muscles only consists of one abductor and one adductor muscle per hip. This simplifies the control model greatly. The abductor and adductor muscular model could be extended by adding more abductor or adductor muscles, instead of lumping them. This could yield better control of the coronal plane, which may lead to reduced oscillations. Furthermore, an interesting research direction would be adding arms to the model. It has been found that arms contribute in reducing the angular momentum after a trip and that a gait with arm swing has a higher perturbation resistance [55], [56]. This increases stability during gait and the ability to counteract perturbations

The simulation for studying fall prevention is not yet realistic enough to be useful. A separate controller for counteracting perturbations should be implemented, such that the controller is able to mimic the fall prevention strategies found in humans. The fall prevention controller should be able to account for a multi-step strategy. Also, the controller should be able to cope with perturbations throughout the whole gait. It would be a good idea to first create a benchmark test, which can be used to test perturbation resistance of models. This benchmark test will give more insight when comparing different controllers.

In general, the numerical sensitivity has to be decreased. If small differences in for instance hardware result in a unsuccessful gait simulation than this reduces the usability of the model. Although, the control gains can be reoptimized so that a successful simulation is obtained. However, this costs time and is undesirable. The integrator blocks in Simulink seem to be one of the sources of numerical sensitivity. Reduced use of these integrator blocks might yield a decreased sensitivity. Also more expertise is needed in the solver settings of Matlab, so that the best settings are used.

Lastly, it would be interesting to do more research and experiments on whether the amputee gait with an added weight or CMG is more symmetric than without. Currently, studies have given an inconclusive answer. If a simple solution such as adding inertial load to the prosthesis could yield a more symmetric gait, than it is worth investigating.

V. Conclusions

The simulated gait of the 3D neuromuscular model of an TF amputee wearing the Otto-bock 3R60 knee prosthesis agrees well with literature. This is especially true when the model walks at $1.2\,\mathrm{m/s}$. For the model walking at the lower velocity, $0.9\,\mathrm{m/s}$, the model deviates more, both for the amputee model, as well as for the healthy model. More research into modeling the muscular structure and neurological control of humans is needed. For the case study on fall prevention, a control moment gyroscope embedded in the prosthetic shank. The resulting simulations show that with an embedded control moment gyroscope, the gait symmetry at $1.2\,\mathrm{m/s}$ is improved. Furthermore, a fall after a trip was successfully prevented using a control moment gyroscope. However, this simulation is numerically very sensitive, so no definitive conclusions can be drawn. For further research into fall prevention using simulation, a fall prevention control model needs to be developed that better resembles human fall prevention strategies.

Acknowledgment

First of all, I would like to thank Prof.dr.ir. H. Vallery, Dr.ir. J. Kober, and ir. Jabeen for their supervision, help, and feedback during the thesis process. Furthermore, I want to thank Prof.dr.ir. D. Rixen for providing the document and Matlab file of the thesis of Vandaele, which contained crucial information for modeling the 3R60 knee prosthesis. Lastly, I want to thank Edwin Verbrugge of Rijndam Orthopedietechniek, who has provided me with a 3R60, which helped in better understanding the knee prosthesis.

Appendix A

Skeletal model

A-1 Skeletal model

The local axes of the body segments are parallel with the global axes, when all the joint angles are zero and the model faced towards positive x-direction. In the model hip extension, hip abduction, knee flexion, and ankle plantarflexion are defined as the positive direction of rotation. When plotting the joint angles, the data is plotted such that hip flexion, hip abduction, knee flexion, and ankle dorsiflexion are positive.

Table A-1: Properties of the different skeletal segments. The local axes of the segments are defined such that they align with the global axis if all joint angles are zero and the model stands straight.

	HAT	Thigh		Shank		Foot	
		Intact	Residual	Intact	Prosthetic	Intact	Prosthetic
mass (kg)	53.5	8.5	7.5	3.5	0.2	1.25	0.55
Length (m)	0.8	0.46	0.35	0.46	0.36	0.2	0.2
Moment of inertia ($\text{kg} \cdot \text{m}^2$)	$\begin{bmatrix} 4 \\ 2.5 \\ 1 \end{bmatrix}$	$\begin{bmatrix} 0.15 \\ 0.15 \\ 0.03 \end{bmatrix}$	$\begin{bmatrix} 0.15 \\ 0.15 \\ 0.03 \end{bmatrix}$	$\begin{bmatrix} 0.05 \\ 0.05 \\ 0.003 \end{bmatrix}$	$\begin{bmatrix} 0.002 \\ 0.002 \\ 0.00012 \end{bmatrix}$	$\begin{bmatrix} 0.0007 \\ 0.005 \\ 0.005 \end{bmatrix}$	$\begin{bmatrix} 0.00023333 \\ 0.0016667 \\ 0.0016667 \end{bmatrix}$

Table A-2: Anatomical joint limits used for the soft joint limit algorithm.

	Hip flexion	Hip abduction	Knee flexion	Ankle flexion
θ_{max} (deg)	-	50	-	20
θ_{min} (deg)	-50	-15	1	-40

Appendix B

Model of the 3R60

B-1 Properties of 3R60 links

In Fig. B-1 a more detailed schematic drawing of the 3R60 knee is shown. All the links have been numbered so that the properties can be given more easily. The lengths, masses, and other properties of the links are given in Table B-2. Vandaele obtained the link properties via 3D CAD drawings provided by Otto Bock [20]. The force in the hydraulic elements is described as

$$F(x(t), \dot{x}(t)) = k(x(t) - x_0) + c\dot{x}(t), \tag{B-1}$$

where F is the hydraulic element force in N, k is the element stiffness in N/m, x is the total length and x_0 the slack length of the element in meters, c is the damping coefficient in Ns/m, and $\dot{x}$ is the element's lengthening velocity in m/s. The properties of the hydraulic elements, are given in Table B-1. These properties are obtained by Vandaele via experiments on both the swing- and stance-phase hydraulic elements [20].

Table B-1: Properties of the hydraulic elements as described in [20]. Link 5 is the stance-phase element, and link 8 is the swing-phase element.

Link number	Slack Length (mm)	Stiffness (kN/m)	Compression Damping $\dot{x} < 0$ (Ns/m)	Extension Damping $\dot{x} > 0$ (Ns/m)
5	89.25	130	$\frac{2.1443\,\text{N}}{\lvert\dot{x}\rvert} + 885.0653\,\text{Ns/m}$	$\frac{7.0819\,\text{N}}{\lvert\dot{x}\rvert} + 65579\,\text{Ns/m}$
8	89.6	18.75	$\frac{213.5932\,\text{N}}{\lvert\dot{x}\rvert} - 4927.5\,\text{Ns/m}$	$\frac{146.3288\,\text{N}}{\lvert\dot{x}\rvert} - 8808.5\,\text{Ns/m}$

[1] Can be used

Table B-2: Properties of the links which make up the 3R60 knee. Every set of rigidly attached links has one (small) link that acts as the center of mass. The center of mass is located at the end of these small 'side' links.

Link number	Length (mm)	Mass (g)	Inertia (kgm^2)	Angle with previous link (°)	Previous link
1	88.5	0	0	18	y-axis
2	1.7	253.3	25.96e−5	−90	1
3	40.25	0	0	−112	1
4	14.9	0	0	−98	1
6	95	0	0	-	-
7	8.2	123.8	1.18e−4	90	6
9	7.9	0	0	-	-
10	3.3	49.5	4.13e−6	−118	9
11	76.95	0	0	-	-
12	3.8	58.3	3.59e−5	−90	11
13	26	0	0	122	16
14	17.7	0	0	116	16
15	1.7	196.6	6.86e−5	34	16
16	25.1	0	0	-	-

B-2 Validation tests details

In order to verify that the model in Simulink resembles the model created by Vandaele, two of his tests were reproduced and the results were compared. The first is the 'release' test and the second is the 'stance phase flexion' test. For the release test the shank connection of the prosthesis is locked, and the rest is free to move. The prosthesis is then released from a certain initial position and the angle θ is tracked in degrees, as shown in Fig. B-2. For the stance phase flexion test a downwards directed sinusoidal force

$$F = 700 \sin\left(\frac{\pi t}{1.5\,\mathrm{s}}\right) \mathrm{N}, \tag{B-2}$$

is exerted on the thigh connection, with the shank connection locked again. This causes the prosthesis to rotate as it would during stance phase, meaning the stance phase hydraulic element is compressed. The stance phase flexion test is visualized in Fig. B-2. During the stance phase flexion test the knee angle φ_k, and the lengths of the hydraulic elements are tracked and calculated.

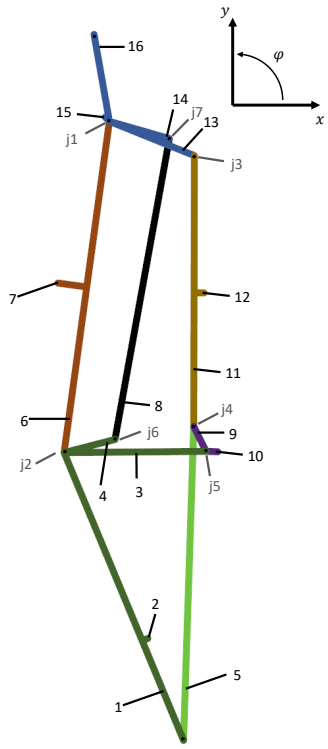

Figure B-1: Schematic drawing of the 3R60 knee prosthesis with numbered links (1-16) and numbered link joints (j1-j7).

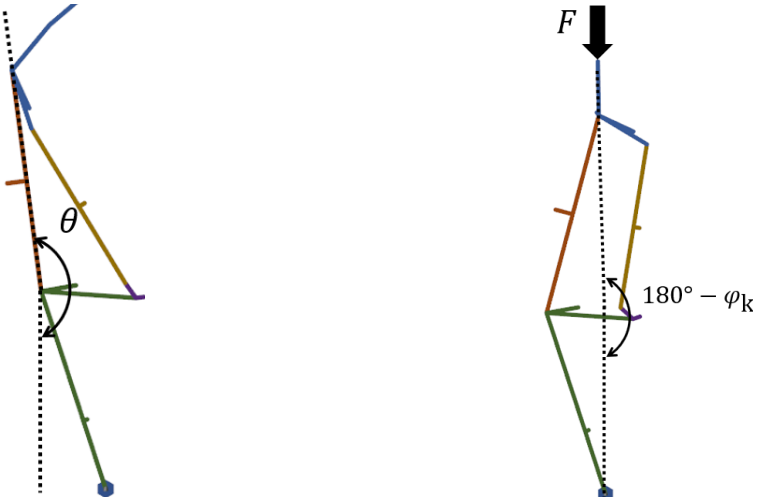

Figure B-2: Two experiments conducted by Vandaele: the release test (left), and the stance phase flexion test (right). In both experiments the shank connection is locked. For the release test the 3R60 is released from the initial position and the angle θ is tracked after release. In the stance phase flexion test a sinusoidal force F is put on the thigh connection resulting in stance phase flexion response of the knee. During this experiment the knee angle φ_{k} is tracked. Note that the hydraulic elements are not shown in this figure.

B-3 Validation tests results

The results of the two tests as executed by Vandaele in [20] are shown in Fig. F-1 and B-4. Fig. F-1 shows the angle θ during the release test for the Simulink model created in this research, the model of Vandaele, and the experiment executed by Vandaele. In Fig. B-4 the results of the stance phase flexion test of the Simulink model are presented. When comparing the results of this test to Figure 12.7 and 12.8 in the thesis of Vandaele [20] it can be seen that the lengths of the hydraulic units differ during the test. First of all the Simulink model flexes more than the model of Vandaele and it extends slower. This means that there are some deviations from the original model by Vandaele, or some initial conditions are unknown which might be crucial for replicating the test. Still, the response during walking shows the characteristics that were expected, such as the stance-phase flexion. So the 3R60 model is assessed to be sufficiently accurate for simulating the trans-femoral (TF) amputee gait.

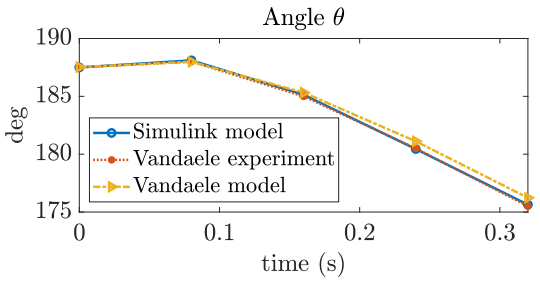

Figure B-3: Angle θ in degrees during the release test, the Simulink model created in this research, the model of Vandaele [20], and the experiment executed by Vandaele.

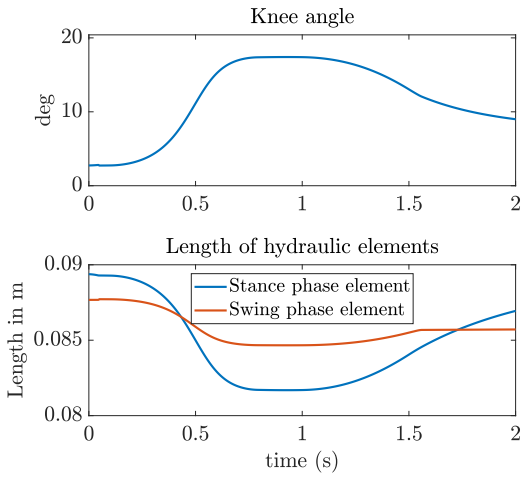

Figure B-4: Knee angle φ_k in degrees, and the length of the hydraulic elements in meters are tracked during the stance phase flexion test. The figure can be compared to Figure 12.7 and 12.8 in [20].

Appendix C

Muscular model

C-1 Muscle-tendon model

The muscle-tendon model of Geyer *et al.* [28] is used. This model is based upon the Hill-type muscle-tendon model. The muscle-tendon model consists of a contractile element (CE), parallel element (PE), series element (SE), and a buffer element (BE). Fig. C-1 shows a schematic overview of how the muscle-tendon unit (MTU) is build up.

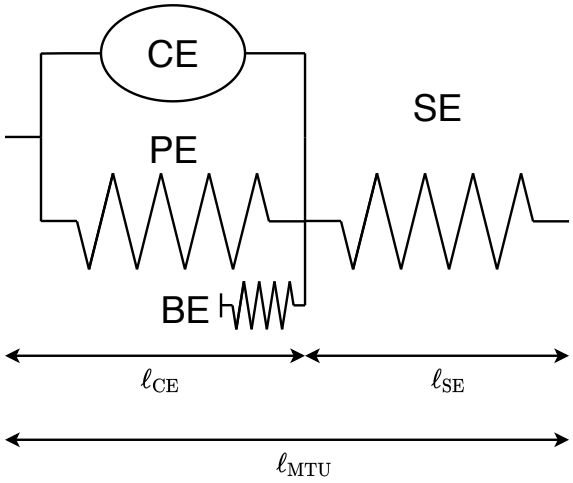

Figure C-1: Muscle-tendon combination as represented by the Hill-type muscle-tendon model

The total force of the muscle-tendon unit F_{MTU} is calculated using

$$F_{\mathrm{MTU}} = F_{\mathrm{SE}} = F_{\mathrm{CE}} + F_{\mathrm{PE}} - F_{\mathrm{BE}}, \tag{C-1}$$

where F_{SE} is the force in the series element (SE), the tendon, F_{CE} is the force in the contractile element (CE), F_{PE} is the force in the parallel element (PE), and F_{BE} is the buffer element

elasticity force. Each separate force can be calculated:

$$\begin{aligned}
F_{\mathrm{CE}} &= F_{\max} \cdot a \cdot f_\ell(\ell_{\mathrm{CE}}) \cdot f_v(v_{\mathrm{CE}}) \\
F_{\mathrm{PE}} &= F_{\max} \cdot \underbrace{\left(\frac{\ell_{\mathrm{CE}} - \ell_{\mathrm{opt}}}{\ell_{\mathrm{opt}} w}\right)^2}_{f_{\mathrm{PE}}} \cdot f_v(v_{\mathrm{CE}}) \cdot (\ell_{\mathrm{CE}} > \ell_{\mathrm{opt}}) \\
F_{\mathrm{BE}} &= F_{\max} \cdot \underbrace{\left(\frac{2\ell_{\mathrm{opt}} - \ell_{\mathrm{CE}} - w}{\ell_{\mathrm{opt}} w}\right)^2}_{f_{\mathrm{BE}}} \cdot (\ell_{\mathrm{MTU}} - \ell_{\mathrm{CE}} < \ell_{\mathrm{slack}}) \\
F_{\mathrm{SE}} &= F_{\max} \cdot \underbrace{\left(\frac{\ell_{\mathrm{SE}} - \ell_{\mathrm{slack}}}{\ell_{\mathrm{slack}} \epsilon_{\mathrm{ref}}}\right)^2}_{f_{\mathrm{SE}}} \cdot (\ell_{\mathrm{SE}} - \ell_{\mathrm{slack}} > 0)
\end{aligned} \tag{C-2}$$

The used parameters are described in Table C-1. The force-length relationship f_ℓ, and the force-velocity relationship f_v are modeled as:

$$f_\ell(\ell_{\mathrm{CE}}) = \exp\left[c\left|\frac{\ell_{\mathrm{CE}} - \ell_{\mathrm{opt}}}{\ell_{\mathrm{opt}} w}\right|^3\right], \tag{C-3}$$

$$f_v(v_{\mathrm{CE}}) = \begin{cases} \dfrac{v_{\max} - v_{\mathrm{CE}}}{v_{\max} + K v_{\mathrm{CE}}} & \text{if } v_{\mathrm{CE}} < 0 \\ N + (N-1)\dfrac{v_{\max} + v_{\mathrm{CE}}}{7.56 K v_{\mathrm{CE}} - v_{\max}} & \text{if } v_{\mathrm{CE}} \geq 0. \end{cases} \tag{C-4}$$

The activation state a is described with a first-order differential equation with the stimulation s as input

$$\tau \frac{\mathrm{d}a}{\mathrm{d}t} = s - a. \tag{C-5}$$

Fig. C-2 and Fig. C-3 show the force of the MTU which depends on the length of both the CE or the SE. The force due to the force-length relationship of the CE is the active force exerted by the muscle. The other forces from the force-length relationships are passive muscle forces. Fig. C-4 shows the force of the CE due to the force-velocity relationship. Table C-2 and Table C-3 show the properties of each muscle used in the model.

Table C-1: Description of the different parameters used for calculating the force of the muscle. These parameters are based on the work of [28]

Parameter	Description
f_ℓ	force-length relationship
f_v	force-velocity relationship
ℓ_{CE}	Length of the CE
v_{CE}	Lengthening velocity of the CE
$v_{\max}$	Maximum lengthening velocity of the CE
ℓ_{opt}	Optimum length for maximum force production of the CE
$F_{\max}$	Maximum force of a muscle
s	Stimulation level of a muscle
a	Activation level of a muscle
w	Width of the bell-shaped f_ℓ curve
ϵ_{ref}	Reference strain of 0.04
c	Constance with value: $\ln(0.05)$, fulfilling $f_\ell(\ell_{\text{opt}}(1 \pm w)) = 0.05$
K	Curvature constant
N	Dimensionless magnitude of force $F_{\text{MTU}}/F_{\max}$ reached at $v_{\text{CE}} = -v_{\max}$

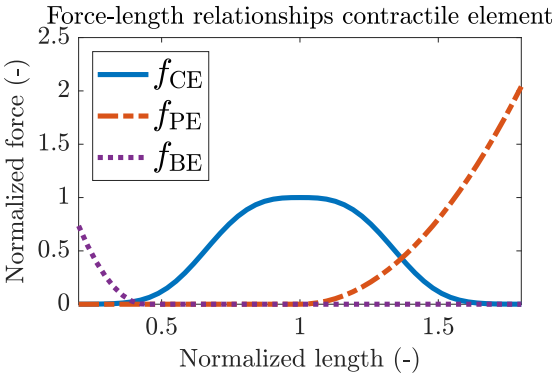

Figure C-2: Force-length curves for the contractile element (CE), parallel element (PE), and buffer element (BE) used in this model from [28]. The force normalized with $F_{\max}$ and the length with ℓ_{opt}.

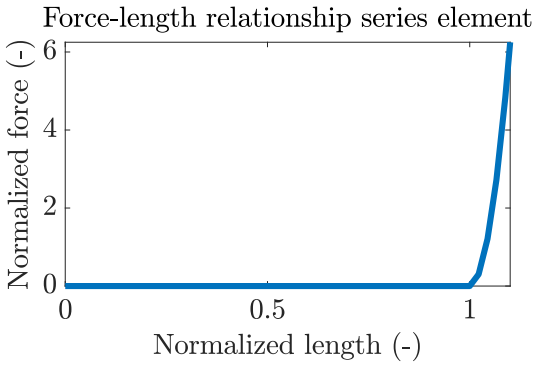

Figure C-3: Force-length curve of the series element (SE) used in this model from [28]. The force is normalized with $F_{\max}$ and the length with ℓ_{opt}.

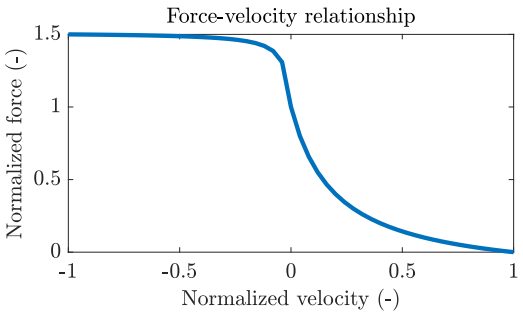

Figure C-4: Force-velocity curve of the contractile element (CE) used in this model from [28]. The force normalized with $F_{\max}$ and the length with $v_{\max}$.

Table C-2: Muscle attachment parameters for all the healthy muscles. Where r_0 is the constant moment arm, $r_{\max}$ and $r_{\min}$ are the maximum and minimum moment arms corresponding to the maximum and minimum joint angle $\varphi_{\max}$ and $\varphi_{\min}$, φ_0 is the reference joint angle when the length of the muscle is equal tot the optimal contractile element (CE) length and the series element (SE) length: $\ell^{\mathrm{m}} = \ell_{\mathrm{opt}} + \ell_{\mathrm{slack}}$. Finally, ρ is the pinnation angle of the muscle-tendon unit (MTU). For the amputated leg muscles the parameters regarding the knee and ankle are unused.

	Hip						Knee					Ankle		
	HAB	HAD	HFL	GLU	HAM	RF	HAM	RF	VAS	BFSH	GAS	GAS	SOL	TA
r_0 (cm)	6	3	8	8	8	8	5	-	-	4	-	-	-	-
$r_{\max}$ (cm)	-	-	-	-	-	-	-	6	6	-	5	6	6	4
$r_{\min}$ (cm)	-	-	-	-	-	-	-	4	4	-	2	2	2	1
$\varphi_{\max}$ (deg)	-	-	-	-	-	-	-	15	15	-	40	10	10	-10
$\varphi_{\min}$ (deg)	-	-	-	-	-	-	-	135	135	-	135	90	90	90
φ_0 (deg)	10	15	-20	-60	-30	-10	0	55	60	20	15	-10	0	20
ρ	70	100	50	50	50	30	50	50	60	70	70	70	50	70

Table C-3: Muscle physiological parameters for both the healthy and amputated leg, where $F_{\max}$ is the maximum muscle force, $v_{\max}$ is the maximum contraction velocity, ℓ_{opt} is the optimal contractile element (CE) length, and ℓ_{slack} is the series element (SE) slack length.

	Healthy leg											Amputated leg					
	HAB	HAD	HFL	GLU	HAM	RF	VAS	BFSH	GAS	SOL	TA	HAB	HAD	HFL	GLU	HAM	RF
$F_{\max}$ (kN)	3	4.5	2	1.5	3	1.2	6	0.35	1.5	4	0.8	2.4	2.7	1.3	0.9	1.8	0.78
$v_{\max}$ (ℓ_{opt}/s)	12	12	12	12	12	12	12	12	12	6	12	12	12	12	12	12	12
ℓ_{opt} (cm)	9	10	11	11	10	8	8	12	5	4	6	9	10	11	11	7.58	6.06
ℓ_{slack} (cm)	7	18	10	13	31	35	23	10	40	26	24	7	18	10	13	23.5	26.53
FT (%)	85	58	50.8	47.6	65.6	62.2	56.3	33.1	49	11	26.6	85	58	50.8	47.6	65.6	62.2

C-2 Muscle expenditure model

A muscle expenditure model is used to give an indication of how much energy it takes to walk a certain gait pattern. In the model of Thatte and Geyer [13] the muscle expenditure model of Umberger [57] is used. However, this model allows the muscle to have a negative metabolic rate resulting from the eccentric work during muscle lengthening, which is not realistic. Umberger has adapted his model and has removed the possibility for a negative metabolic rate [36]. This updated version is used in this work. The muscle expenditure $\dot{E}$ is modeled as a combination of the work rate, $\dot{W}_{\mathrm{CE}}$, the heat rates resulting from activation, $\dot{H}_{\mathrm{A}}$, maintenance of contraction, $\dot{H}_{\mathrm{M}}$, and muscle shortening and lengthening $\dot{H}_{\mathrm{SL}}$. The metabolic energy E_{m} is used in the cost function and is calculated by integrating the energy expenditure:

$$E_{\mathrm{m}} = \int \dot{E}\,\mathrm{d}\,t = \int \left(\dot{H}_{\mathrm{A}} + \dot{H}_{\mathrm{M}} + \dot{H}_{\mathrm{SL}} + \dot{W}_{\mathrm{CE}}\right)\mathrm{d}\,t. \tag{C-6}$$

If the elements of the expenditure model are divided by the muscle weight, the weight independent muscle expenditure becomes:

$$\frac{\dot{E}}{m} = \dot{h}_{\mathrm{A}} + \dot{h}_{\mathrm{M}} + \dot{h}_{\mathrm{SL}} + \dot{w}_{\mathrm{CE}}. \tag{C-7}$$

For calculating the muscle expenditure, the percentage of fast-twitch or slow-twitch muscle fibers in a muscle is needed. These values were based on the findings of Johnson *et al.* [**?**]. In Equations (C-8)-(C-13) the calculations for the expenditure model are described. When $\{\}^{-/+}$ is used, it means that only negative, or positive values are taken into account.

The heat rate due to activation $\dot{h}_{\mathrm{A}}$ and maintenance $\dot{h}_{\mathrm{M}}$ is described in a combined factor $\dot{h}_{\mathrm{AM}}$:

$$\dot{h}_{\mathrm{A}} + \dot{h}_{\mathrm{M}} = \dot{h}_{\mathrm{AM}} = 1.28\,\mathrm{W/kg} \cdot f_{\mathrm{FT}} + 25\,\mathrm{W/kg}. \tag{C-8}$$

where $f_{\mathrm{FT}} = \dfrac{\mathrm{FT}}{100\,\%}$ is the factor of fast twitch fibers in the muscle. The mechanical work work rate $\dot{w}_{\mathrm{CE}}$ is described as

$$\dot{w}_{\mathrm{CE}} = \left\{-\frac{F_{\mathrm{CE}} v_{\mathrm{CE}}}{m}\right\}^{+}, \tag{C-9}$$

and can only be positive.

The heat rate due to shortening and lengthening $\dot{h}_{\mathrm{SL}}$ is described by:

$$\dot{h}_{\mathrm{SL}} = -\alpha_{\mathrm{S(ST)}}\widetilde{v}_{\mathrm{CE}}(1 - f_{\mathrm{FT}}) - \alpha_{\mathrm{S(FT)}}\widetilde{v}_{\mathrm{CE}}(f_{\mathrm{FT}}), \tag{C-10}$$

where $\alpha_{\mathrm{S(ST)}}$ is

$$\alpha_{\mathrm{S(ST)}} = \frac{4 \cdot 25\,\mathrm{W/kg}}{\widetilde{v}_{\mathrm{CE(max_{ST})}}} \tag{C-11}$$

and $\alpha_{\mathrm{S(FT)}}$ is

$$\alpha_{\mathrm{S(FT)}} = \frac{1 \cdot 153\,\mathrm{W/kg}}{\widetilde{v}_{\mathrm{CE(max_{FT})}}}. \tag{C-12}$$

The variables $\widetilde{v}_{\mathrm{CE}}$, $\widetilde{v}_{\mathrm{CE(max_{ST})}}$ and $\widetilde{v}_{\mathrm{CE(max_{FT})}}$ are the muscle contractile velocity, the maximum contractile velocity of the slow twitch fibers, and the maximum contractile velocity of the fast twitch fibers divided by ℓ_{opt}. Furthermore, it is assumed that $\widetilde{v}_{\mathrm{CE(max_{FT})}} = 2.5\widetilde{v}_{\mathrm{CE(max_{ST})}}$

Since $\dot{h}_{\mathrm{AM}}$ and $\dot{h}_{\mathrm{SL}}$ have a dependency on length and activation scaling factors are added. Including this in the total energy, it then is defined as

$$\begin{aligned}
&\text{if } \ell_{\mathrm{CE}} \leq \ell_{\mathrm{opt}} \\
&\frac{\dot{E}}{m} = \dot{h}_{\mathrm{AM}} A_{\mathrm{AM}} S + \dot{w}_{\mathrm{CE}} \\
&+ \begin{cases} \left[-\alpha_{\mathrm{S(ST)}} \widetilde{v}_{\mathrm{CE}} (1 - f_{\mathrm{FT}}) - \alpha_{S(\mathrm{FT})} \widetilde{v}_{\mathrm{CE}} f_{\mathrm{FT}} \right] A_S S & \text{if } \widetilde{v}_{\mathrm{CE}} \leq 0 \\ \alpha_{\mathrm{L}} \widetilde{v}_{\mathrm{CE}} A S & \text{if } \tilde{v}_{\mathrm{CE}} > 0 \end{cases} \\
&\text{if } \ell_{\mathrm{CE}} > \ell_{\mathrm{opt}} \\
&\frac{\dot{E}}{m} = \left(0.4 \dot{h}_{\mathrm{AM}} + 0.6 \dot{h}_{\mathrm{AM}} (-f_{\mathrm{PE}}) \right) A_{\mathrm{AM}} S + \dot{w}_{\mathrm{CE}} \\
&+ \begin{cases} \left[-\alpha_{\mathrm{S(ST)}} \widetilde{v}_{\mathrm{CE}} (1 - f_{\mathrm{FT}}) - \alpha_{\mathrm{S(FT)}} \widetilde{v}_{\mathrm{CE}} f_{\mathrm{FT}} \right] (-f_{\mathrm{PE}}) A_S S & \text{if } \widetilde{v}_{\mathrm{CE}} \leq 0 \\ \alpha_{\mathrm{L}} \tilde{v}_{\mathrm{CE}} (-f_{\mathrm{PE}}) A S & \text{if } \tilde{v}_{\mathrm{CE}} > 0 \end{cases} \\
&\alpha_{\mathrm{L}} = 0.3 \cdot \alpha_{\mathrm{S(ST)}} \quad A_{\mathrm{S}} = a^2, \quad A_{\mathrm{AM}} = a^{0.6}, \quad S = 1.5.
\end{aligned} \tag{C-13}$$

The parameters F_{CE}, v_{CE}, and ℓ_{CE} are the force, velocity and length of the of the CE of the muscle and ℓ_{opt} is its optimal length. The scaling factors A, A_S, and A_{AM} account for a different heat liberation between aerobic and anaerobic activity and S is a scaling factor for aerobic conditions.

Appendix D

Control moment gyroscope model and control

D-1 Model

Fig. D-1 shows the model of the control moment gyroscope (CMG) with the definitions of the distance from the shank center of mass (COM) d, the radius of the CMG r, and the thickness of the CMG h visualized as well.

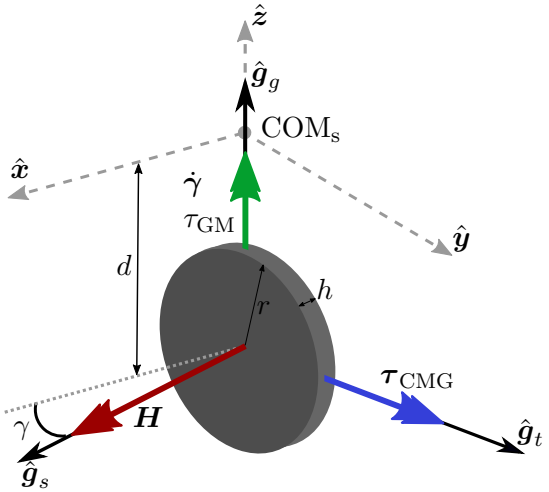

Figure D-1: Model of the control moment gyroscope (CMG), as earlier explained in Subsection II-E. CMG radius r, thickness h, and distance from the shank center of mass (COM) d are shown in the figure.

The inertia of the CMG is assumed to be the sum of the inertia of a point mass that has a mass half the total mass of the CMG and is located at a distance r from the center, and of a solid cylinder with radius r with also a mass equal to half the total CMG mass. The moment

of inertia around the $\hat{\boldsymbol{g}}_s$ axis I_{ss} is

$$I_{ss} = \frac{m}{2}r^2 + \frac{1}{2}\frac{m}{2}r^2 = \frac{3}{4}mr^2 = 1.2\text{e}{-3}\,\text{kgm}^2. \tag{D-1}$$

The moment of inertia around the $\hat{\boldsymbol{g}}_t$ and $\hat{\boldsymbol{g}}_g$ axis are equal

$$I_{tt} = I_{gg} = \frac{1}{12}\frac{m}{2}(6r^2 + h^2) + \frac{1}{12}\frac{m}{2}(3r^2 + h^2) = \frac{m}{12}(3r^2 + h^2) + \frac{m}{8}^2 = 6.02\text{e}{-4}\,\text{kgm}^2. \tag{D-2}$$

When $\gamma = 0$ the inertia matrix becomes

$$\mathbf{I}_{\text{C}_0} = \begin{bmatrix} I_{ss} & 0 & 0 \\ 0 & I_{tt} & 0 \\ 0 & 0 & I_{gg} \end{bmatrix}. \tag{D-3}$$

The neutral angle for the CMG, however, was set to $-70\,^\circ$. This was found to be working well, since it reduces the parasitic moments due to knee flexion, but does not totally remove controllability in the sagittal plane. Then the inertia matrix aligned with the local shank axes is

$$\mathbf{I}_{\text{C}_{\gamma_0}} = \mathbf{R}_{\gamma_0}\mathbf{I}_{\text{C}_0}\mathbf{R}_{\gamma_0}^{\text{T}}, \tag{D-4}$$

where

$$\mathbf{R}_{\gamma_0} = \begin{bmatrix} \cos(-70\,^\circ) & -\sin(-70\,^\circ) & 0 \\ \sin(-70\,^\circ) & \cos(-70\,^\circ) & 0 \\ 0 & 0 & 1 \end{bmatrix}. \tag{D-5}$$

D-2 Controller

The torque exerted on the shank is a result from the gyroscopic torque of the CMG. A gyroscopic torque is created if the CMG has angular momentum $\boldsymbol{H}$ and angular velocity of the gimbal motor (GM) $\dot{\boldsymbol{\gamma}}$, or the shank $\boldsymbol{\omega}_\text{s}$. This torque results in a reaction torque on the shank $\boldsymbol{\tau}_\text{s}$. This reaction torque on the shank can be split up into different components, namely an anterior-posterior τ_AP, a medio-lateral τ_ML, and a longitudal τ_L component:

$$\begin{aligned}
\boldsymbol{\tau}_\text{s}(t) &= -\boldsymbol{\tau}_\text{CMG}(t) \\
\boldsymbol{\tau}_\text{s}(t) &= -\dot{\boldsymbol{H}}(t) \\
&= -(\dot{\boldsymbol{\gamma}}(t) + \boldsymbol{\omega}_\text{s}(t)) \times \boldsymbol{H}(t) - \boldsymbol{\tau}_\text{GM}(t) \\
&= -\begin{bmatrix} \omega_{\hat{\boldsymbol{x}}}(t) \\ \omega_{\hat{\boldsymbol{y}}}(t) \\ \dot{\gamma}(t) + \omega_{\hat{\boldsymbol{z}}}(t) \end{bmatrix} \times I_\text{ss}\Omega \begin{bmatrix} \cos(\gamma(t)) \\ \sin(\gamma(t)) \\ 0 \end{bmatrix} - \begin{bmatrix} 0 \\ 0 \\ \tau_\text{GM}(t) \end{bmatrix} \\
&= \begin{bmatrix} I_\text{ss}\Omega(\dot{\gamma}(t) + \omega_{\hat{\boldsymbol{z}}}(t))\sin(\gamma(t)) \\ -I_\text{ss}\Omega(\dot{\gamma}(t) + \omega_{\hat{\boldsymbol{z}}}(t))\cos(\gamma(t)) \\ I_\text{ss}\Omega(\omega_{\hat{\boldsymbol{y}}}\cos(\gamma(t)) - \omega_{\hat{\boldsymbol{x}}}(t)\sin(\gamma(t))) - \tau_\text{GM}(t) \end{bmatrix} \\
&= \tau_\text{ML}(t)\hat{\boldsymbol{x}} + \tau_\text{AP}(t)\hat{\boldsymbol{y}} + \tau_\text{L}(t)\hat{\boldsymbol{z}}
\end{aligned} \tag{D-6}$$

The total gimbal motor torque applied is determined by

$$\begin{aligned}\tau_{\mathrm{GM}}(t) = I_{\mathrm{ss}}\Omega(\omega_{\hat{\boldsymbol{y}}}\cos(\gamma(t)) - \omega_{\hat{\boldsymbol{x}}}(t)\sin(\gamma(t))) \\ + \begin{cases}\tau_{\mathrm{w}}(t), & \text{if walking} \\ \tau_{\mathrm{f}}(t), & \text{if trip.}\end{cases}\end{aligned} \tag{D-7}$$

It consists of a feedforward , which comes from the longitudal gyroscopic torque component, a 'walk controller' τ_{w}, and a 'fall prevention controller' τ_{f} term. The walk controller minimizes parasitic moments during walking. This is done by setting the desired angular velocity of the gimbal motor opposite to the angular velocity $\omega_{\hat{\boldsymbol{z}}}$ of the $\hat{\boldsymbol{z}}$-axis: $\dot{\gamma}(t) = -\omega_{\hat{\boldsymbol{z}}}(t)$. This cancels the parasitic moment in the anterior-posterior, and medio-lateral directions. During stance the controller lets the gimbal axis return to the initial position γ_0. The torque applied by the controller is:

$$\tau_{\mathrm{w}}(t) = \begin{cases}\tau_{\mathrm{L}}\left(t, -\omega_{\hat{\boldsymbol{z}}}(t)\right), & \text{if swing} \\ -k_{p0}(\gamma_0 - \gamma(t)) - k_{d0}\dot{\gamma}(t), & \text{if stance.}\end{cases} \tag{D-8}$$

The parameters $k_{p0} = 150\,\mathrm{Nm/rad}$, $k_{d0} = 40\,\mathrm{Nms/rad}$ are the proportional and derivative gains of the controller. As said previously, the neutral angle of the CMG γ_0 is set to $-70\,\mathrm{deg}$.

A low-level proportional-integral controller determines the amount of torque for tracking the desired angular velocity of the gimbal motor

$$\tau_{\mathrm{L}}(t, \dot{\gamma}_{\mathrm{ref}}) = k_p e_{\dot{\gamma}}(t) + k_i \int e_{\dot{\gamma}}(t)\,\mathrm{d}\,t \tag{D-9}$$

$$e_{\dot{\gamma}}(t) = \dot{\gamma}_{\mathrm{ref}}(t) - \dot{\gamma}(t). \tag{D-10}$$

The low-level controller gains are: $k_p = 20\,\mathrm{Nms/rad}$, $k_i = 1\,\mathrm{Nm/rad}$. The fall prevention controller applies a torque τ_{t}, such that a desired gyroscopic torque is created.

The fall prevention controller algorithm calculates a desired shank torque in anterior-posterior direction τ_{APr} to aid the recovery step. The desired shank torque is determined by

$$\begin{aligned}\tau_{\mathrm{APr}}(t) = -I_{\mathrm{ss}}\Omega\omega_{\hat{\boldsymbol{z}}}(t)\cos(\gamma(t)) \\ + \begin{cases}k_{p,\mathrm{s}}(\alpha_{\mathrm{ref}}(t) + \Delta_\alpha - \alpha(t)) \cdot (1 - \frac{\dot{\alpha}(t)}{\dot{\alpha}_{\max}}) - & \text{if } \ell_{\mathrm{L}}(t) < \ell_{\mathrm{L,c}} \\ k_{p,\mathrm{e}}(\ell_{\mathrm{L,c}} - \ell_{\mathrm{L}}(t)) & \textit{and} \text{ contrastance } \textit{and} \text{ !stance} \\ & (\alpha_{\mathrm{ref}}(t) + \Delta_\alpha > \alpha(t)) \textit{and } (\dot{\alpha}(t) < \dot{\alpha}_{\max}) \\ k_{p,\alpha}(\alpha_{\mathrm{ref,t}} - \alpha(t)) - k_{p,\dot{\alpha}}\{\dot{\alpha}(t)\}_- & \text{otherwise.}\end{cases}\end{aligned} \tag{D-11}$$

The parameters $k_{p,\mathrm{s}}$ is a gain which causes the leg to stop rotating when the leg angle α is within a threshold Δ_α of the target leg angle α_{ref}, and if the maximum leg angle velocity $\dot{\alpha}$ is below the maximum leg angle velocity $\dot{\alpha}_{\max}$. This means it decreases knee flexion velocity. The parameters $k_{p,\mathrm{e}}$ does the opposite, it causes the knee to extend if the leg length ℓ_{L} is above a certain clearance leg length $\ell_{\mathrm{L,c}}$. So this first part of the fall prevention controller makes sure that the leg does not rotate too far, and extends when it is possible. The second part of the controller is meant for making sure that at the start of fall prevention there is

enough ground clearance. It does this by flexing the knee. The gain $k_{p,\alpha}$ is a proportional gain of the difference between the leg angle and a set reference leg angle during the start of fall prevention $\alpha_{\text{ref,t}}$. The parameter $k_{p,\dot{\alpha}}$ makes sure the target leg angle velocity is positive to ensure increasing the leg clearance. This desired shank torque is then converted into to a desired angular velocity of the gimbal motor:

$$\tau_{\text{f}}(t) = \tau_{\text{L}}\left(t, \dot{\gamma}_{\text{ref}}(t)\right) \tag{D-12}$$

$$\dot{\gamma}_{\text{ref}}(t) = \frac{-\tau_{\text{APr}}(t)}{I_{\text{ss}}\Omega\cos\left(\gamma(t)\right)} - \omega_{\hat{z}}(t), \tag{D-13}$$

which is fed into the low-level controller to track the desired angular velocity of the gimbal axis. The values for the fall prevention controller gains are: $k_{p,\text{s}} = 2299\,\text{Nm/rad}$, $k_{p,\text{e}} = 834\,\text{N}$, $k_{p,\alpha} = 0.006\,\text{Nm/rad}$, $k_{p,\dot{\alpha}} = 4.7e05\,\text{Nms/rad}$, $\alpha_{\text{ref,t}} = 26.6\,\text{rad}$, $\ell_{\text{L,c}} = 1.70\,\text{m}$.

D-2-1 Natural frequencies

Calculating the natural frequency ω_n of a pendulum-like rigid body can be done using

$$\omega_n = \sqrt{\frac{mgd}{I}}, \tag{D-14}$$

where m is the mass of the rigid body, g the gravity constant, d the distance of the COM to the reference point, and I the moment of inertia around the reference point. The natural frequencies of the healthy shank-foot combination ω_{H}, the prosthetic shank-foot ω_{P}, and the prosthetic shank-foot with CMG ω_{C} are calculated. First the inertia around, and the distance to the reference point have to be calculated. In this case the reference point is the knee. Also for the prosthetic leg the reference point is the location where the intact knee would be. This is a simplification, because the instantaneous center of rotation (ICR) of the 3R60 changes during knee movement.

The moment of inertia of the healthy shank-foot around the knee joint is calculated using the parallel-axis theorem

$$\begin{aligned} I_{\text{H},y} &= I_{\text{s},y} + m_{\text{s}} \cdot d_{\text{s}}^2 + I_{\text{f},y} + m_{\text{f}} \cdot d_{\text{f}}^2 \\ &= 0.05\,\text{kgm}^2 + 3.5\,\text{kg} \cdot (0.2\,\text{m})^2 + 0.005\,\text{kgm}^2 + 1.25\,\text{kg} \cdot (0.4\,\text{m})^2 = 0.46\,\text{kgm}^2, \end{aligned} \tag{D-15}$$

where $I_{\text{s},y}$ is the moment of inertia of the shank around its COM, d_{s} is the distance from the COM of the shank to the knee, $I_{\text{f},y}$ is the moment of inertia of the foot around its COM, d_{f} is the distance from the COM of the foot to the knee, and m_{s} and m_{f} are the masses of the shank and foot. The distance from the knee joint to the COM of the healthy shank-foot combination is

$$\begin{aligned} d_{\text{H}} &= \frac{m_{\text{s}} \cdot d_{\text{s}} + m_{\text{f}} \cdot d_{\text{f}}}{m_{\text{s}} + m_{\text{f}}} \\ &= \frac{3.5\,\text{kg} \cdot 0.2\,\text{m} + 1.25\,\text{kg} \cdot 0.46\,\text{m}}{3.5\,\text{kg} + 1.25\,\text{kg}} = 0.27\,\text{m}. \end{aligned} \tag{D-16}$$

Then the natural frequency of the healthy shank-foot combination is

$$\begin{aligned}\omega_{\mathrm{H}} &= \sqrt{\frac{(m_{\mathrm{s}} + m_{\mathrm{f}}) \cdot g \cdot d_{\mathrm{H}}}{I_{\mathrm{H}}}} \\ &= \sqrt{\frac{(3.5\,\mathrm{kg} + 1.25\,\mathrm{kg}) \cdot 9.81\,\mathrm{ms}^2 \cdot 0.27\,\mathrm{m}}{0.46\,\mathrm{kgm}^2}} = 5.22\,\mathrm{rad/s}.\end{aligned} \tag{D-17}$$

The moment of inertia of the prosthetic shank-foot around the knee joint is

$$\begin{aligned}I_{\mathrm{P},y} &= I_{\mathrm{ps},y} + m_{\mathrm{ps}} \cdot d_{\mathrm{ps}}^2 + I_{\mathrm{f},y} + m_{\mathrm{pf}} \cdot d_{\mathrm{pf}}^2 \\ &= 0.002\,\mathrm{kgm}^2 + 0.2\,\mathrm{kg} \cdot (0.2\,\mathrm{m})^2 + 0.0017\,\mathrm{kgm}^2 + 0.55\,\mathrm{kg} \cdot (0.46\,\mathrm{m})^2 = 0.13\,\mathrm{kgm}^2.\end{aligned} \tag{D-18}$$

where $I_{\mathrm{ps},y}$ is the moment of inertia of the prosthetic shank around its COM, d_{ps} is the distance from the COM of the prosthetic shank to the knee, $I_{\mathrm{pf},y}$ is the moment of inertia of the prosthetic foot around its COM, and d_{pf} is the distance from the COM of the prosthetic foot to the knee. The masses of the prosthetic shank and foot are denoted by $m_{\mathrm{ps}}, m_{\mathrm{pf}}$. The distance from the knee joint to the COM of the prosthetic shank-foot combination is

$$\begin{aligned}d_{\mathrm{P}} &= \frac{m_{\mathrm{ps}} \cdot d_{\mathrm{ps}} + m_{\mathrm{pf}} \cdot d_{\mathrm{pf}}}{m_{\mathrm{ps}} + m_{\mathrm{pf}}} \\ &= \frac{0.2\,\mathrm{kg} \cdot 0.2\,\mathrm{m} + 0.55\,\mathrm{kg} \cdot 0.46\,\mathrm{m}}{0.2\,\mathrm{kg} + 0.55\,\mathrm{kg}} = 0.39\,\mathrm{m}.\end{aligned} \tag{D-19}$$

Then the natural frequency of the prosthetic shank-foot combination is

$$\begin{aligned}\omega_{\mathrm{P}} &= \sqrt{\frac{(m_{\mathrm{ps}} + m_{\mathrm{pf}}) \cdot g \cdot d_{\mathrm{P}}}{I_{\mathrm{P}}}} \\ &= \sqrt{\frac{(0.2\,\mathrm{kg} + 0.55\,\mathrm{kg}) \cdot 9.81\,\mathrm{ms}^2 \cdot 0.39\,\mathrm{m}}{0.13\,\mathrm{kgm}^2}} = 4.74\,\mathrm{rad/s}.\end{aligned} \tag{D-20}$$

The moment of inertia of the prosthetic shank-foot with CMG around the knee joint is

$$\begin{aligned}I_{\mathrm{C}} &= I_{\mathrm{P}} + I_{\mathrm{C}_{\gamma_0},y} + m_{\mathrm{CMG}} \cdot d_{\mathrm{CMG}}^2 \\ &= 0.13\,\mathrm{kgm}^2 + 0.0011\,\mathrm{kgm}^2 + 1\,\mathrm{kg} \cdot (0.25\,\mathrm{m})^2 = 0.19\,\mathrm{kgm}^2.\end{aligned} \tag{D-21}$$

where d_{CMG} is the distance from the COM of the CMG to the knee, and m_{CMG} is the mass of the CMG. The distance from the knee joint to the COM of the prosthetic shank-foot combination is

$$\begin{aligned}d_{\mathrm{C}} &= \frac{m_{\mathrm{ps}} \cdot d_{\mathrm{ps}} + m_{\mathrm{pf}} \cdot d_{\mathrm{pf}} + m_{\mathrm{CMG}} \cdot d_{\mathrm{CMG}}}{m_{\mathrm{ps}} + m_{\mathrm{pf}} + m_{\mathrm{CMG}}} \\ &= \frac{0.2\,\mathrm{kg} \cdot 0.2\,\mathrm{m} + 0.55\,\mathrm{kg} \cdot 0.46\,\mathrm{m} + 1\,\mathrm{kg} \cdot 0.25\,\mathrm{m}}{0.2\,\mathrm{kg} + 0.55\,\mathrm{kg} + 1\,\mathrm{kg}} = 0.31\,\mathrm{m}.\end{aligned} \tag{D-22}$$

Then the natural frequency of the prosthetic shank-foot with CMG combination is

$$\begin{aligned}\omega_{\mathrm{C}} &= \sqrt{\frac{(m_{\mathrm{ps}} + m_{\mathrm{pf}} + m_{\mathrm{CMG}}) \cdot g \cdot d_{\mathrm{C}}}{I_{\mathrm{C}}}} \\ &= \sqrt{\frac{(0.2\,\mathrm{kg} + 0.55\,\mathrm{kg} + 1\,\mathrm{kg}) \cdot 9.81\,\mathrm{ms}^2 \cdot 0.31\,\mathrm{m}}{0.19\,\mathrm{kgm}^2}} = 5.27\,\mathrm{rad/s}.\end{aligned} \tag{D-23}$$

Appendix E

Optimization details

E-1 Self collision algorithm

In order to determine whether a collision is occurring between two segments of both legs, the shortest distance between the segments is calculated first. This is done by calculating the distance between two skew lines. Let $\boldsymbol{x}_{1,1}$ be the position of one end of segment 1 and $\boldsymbol{x}_{1,2}$ the position of other end of segment 1. Then $\boldsymbol{x}_{2,1}$ is the position of one end of segment 2 and $\boldsymbol{x}_{2,2}$ the position of the other end of segment 2. Then the direction vectors of each segment are

$$\boldsymbol{e}_1 = \boldsymbol{x}_{1,2} - \boldsymbol{x}_{1,1} \tag{E-1}$$

$$\boldsymbol{e}_2 = \boldsymbol{x}_{2,2} - \boldsymbol{x}_{2,1}. \tag{E-2}$$

The cross product between the two direction vectors is defined as $\boldsymbol{n}$:

$$\boldsymbol{n} = \boldsymbol{e}_1 \times \boldsymbol{e}_2, \tag{E-3}$$

which is perpendicular to both $\boldsymbol{e}_1$ and $\boldsymbol{e}_2$. Then the point of segment 1 that is closest to segment 2 is

$$t_1 = \frac{(\boldsymbol{x}_{2,1} - \boldsymbol{x}_{1,1}) \cdot (\boldsymbol{e}_2 \times \boldsymbol{n})}{\boldsymbol{e}_1 \cdot (\boldsymbol{e}_2 \times \boldsymbol{n})} \tag{E-4}$$

This is the ratio of the projection of the direction vector of $(\boldsymbol{x}_{2,1} - \boldsymbol{x}_{1,1})$ onto $(\boldsymbol{e}_2 \times \boldsymbol{n})$ with the projection of the direction vector of line 1 $\boldsymbol{e}_1$ onto $(\boldsymbol{e}_2 \times \boldsymbol{n})$. Of course the closest point of line 1 to line 2 $\boldsymbol{c}_1$ has to lie within the line itself. If not, then the closest point is either of the ends

$$\boldsymbol{c}_1 = \begin{cases} \boldsymbol{x}_{1,1} & \text{, if } t_1 < 0 \\ \boldsymbol{x}_{1,2} & \text{, if } t_1 > 1 \\ \boldsymbol{x}_{1,1} + t_1 \boldsymbol{e}_1 & \text{otherwise.} \end{cases} \tag{E-5}$$

The point of segment 2 that is closest to segment 1 is

$$t_2 = \frac{(\boldsymbol{x}_{1,1} - \boldsymbol{x}_{2,1}) \cdot (\boldsymbol{e}_1 \times \boldsymbol{n})}{\boldsymbol{e}_2 \cdot (\boldsymbol{e}_1 \times \boldsymbol{n})} \tag{E-6}$$

This is the ratio of the projection of the direction vector of $(\boldsymbol{x}_{1,1} - \boldsymbol{x}_{2,1})$ onto $(\boldsymbol{e}_1 \times \boldsymbol{n})$ with the projection of the direction vector of line 1 $\boldsymbol{e}_2$ onto $(\boldsymbol{e}_1 \times \boldsymbol{n})$. Again, the closest point of line 2 to line 1 $\boldsymbol{c}_2$ has to lie within the line itself. If not, then the closest point is either of the ends

$$\boldsymbol{c}_2 = \begin{cases} \boldsymbol{x}_{2,1} & \text{, if } t_2 < 0 \\ \boldsymbol{x}_{2,2} & \text{, if } t_2 > 1 \\ \boldsymbol{x}_{2,1} + t_2 \boldsymbol{e}_2 & \text{, otherwise.} \end{cases} \tag{E-7}$$

Then the distance d between segment 1 and 2 is the euclidean distance between these two points

$$d = ||\boldsymbol{c}_1 - \boldsymbol{c}_2||. \tag{E-8}$$

A collision is detected if this distance is below a threshold ϵ. In this model $\epsilon = 0.02\,\text{m}$. In the model every segment of the left or intact leg is checked with every segment of the right or prosthetic leg, to make sure that no collision is happening.

E-2 Rough terrain

During optimization of the gait, the model is walking over one flat surface and three rough terrains. For the rough terrain the first 10 m are still flat. After the 10 m random height changes are generated which are scaled such that the maximum height change is 1 cm. Fig. E-1 shows an example of such a generated rough terrain.

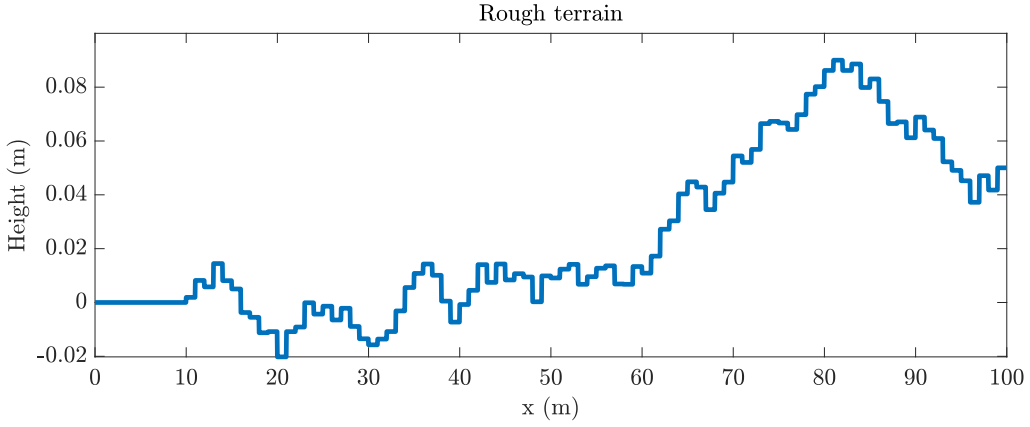

Figure E-1: An example of a generated rough terrain used for gait evaluation during optimization. The first 10 m are flat after which random height changes are generated every meter. These height changes are scaled such that the maximum height change is 1 cm.

Appendix F

Extra results

F-1 Amputee gait

Fig. F-1 to Fig. F-8 show figures providing extra information on the results. For all gait data sets the average values are given. For the simulated gait, the standard deviation is plotted as well. Fig. F-1 and Fig. F-2 show the average joint torque, Fig. F-3 and Fig. F-4 show the average joint power, Fig. F-5 and Fig. F-6 show the average ground reaction forces (GRF), and Fig. F-7 and Fig. F-8 show the average muscle activation level during a stride.

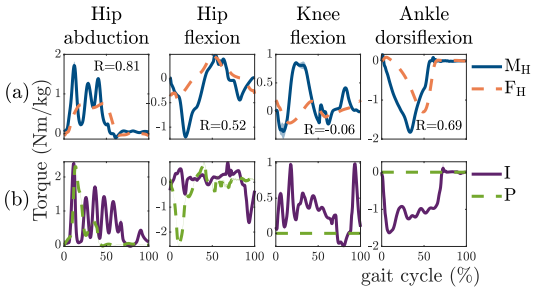

Figure F-1: Average joint torques and standard deviation during a stride of (a) a healthy model (M_H) compared to data from Fukuchi (F_H) [46] and (b) for the intact (I) and prosthetic (P) leg of the amputee model walking on a flat ground with $0.9\,\mathrm{m/s}$, normalized with the body mass.

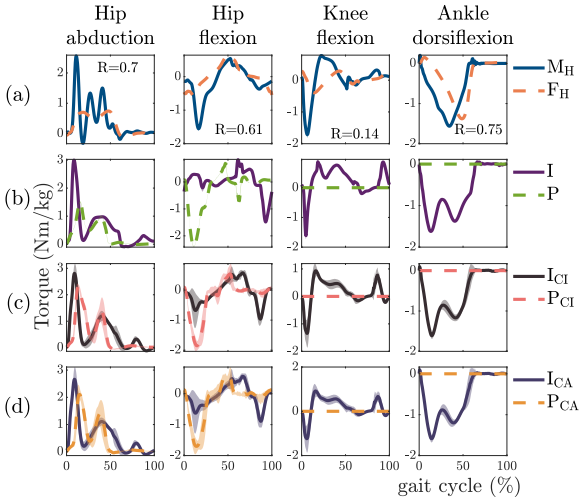

Figure F-2: Average joint torques and standard deviation during a stride of (a) a healthy model (M_H) compared to data from Fukuchi (F_H) [46], and (b) for the intact (I) and prosthetic (P) leg, and (c) for the intact (I_{CI}) and prosthetic (P_{CI}) with inactive control moment gyroscope (CMG), and (d) for the intact (I_{CA}) and prosthetic (P_{CA}) leg with active CMG of the amputee model walking on a flat ground with $1.2\,\mathrm{m/s}$, normalized with the body mass.

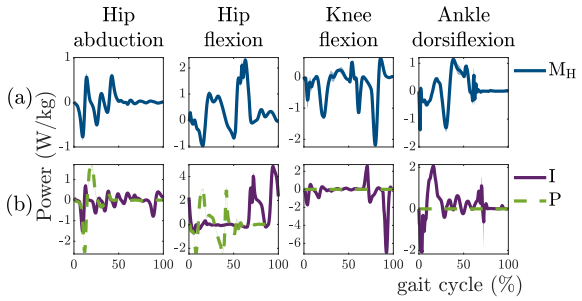

Figure F-3: Average joint powers and standard deviation during a stride of (a) a healthy model (M_H) compared to data from Fukuchi (F_H) [46] and (b) for the intact (I) and prosthetic (P) leg of the amputee model walking on a flat ground with $0.9\,\mathrm{m/s}$, normalized with the body mass.

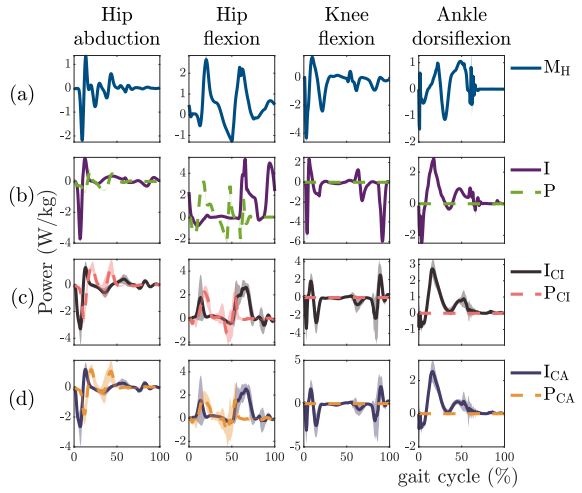

Figure F-4: Average joint powers and standard deviation during a stride of (a) a healthy model (M_H) compared to data from Fukuchi (F_H) [46], and (b) for the intact (I) and prosthetic (P) leg, and (c) for the intact (I_{CI}) and prosthetic (P_{CI}) with inactive CMG, and (d) for the intact (I_{CA}) and prosthetic (P_{CA}) leg with active CMG of the amputee model walking on a flat ground with $1.2\,\mathrm{m/s}$, normalized with the body mass.

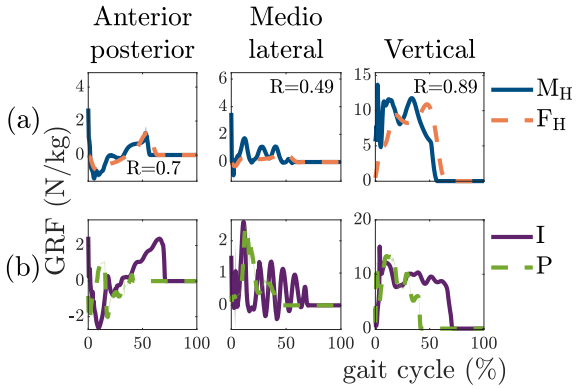

Figure F-5: Average ground reaction forces and standard deviation during a stride of (a) a healthy model (M_H) compared to data from Fukuchi (F_H) [46] and (b) for the intact (I) and prosthetic (P) leg of the amputee model walking on a flat ground with $0.9\,\mathrm{m/s}$, normalized with the body mass.

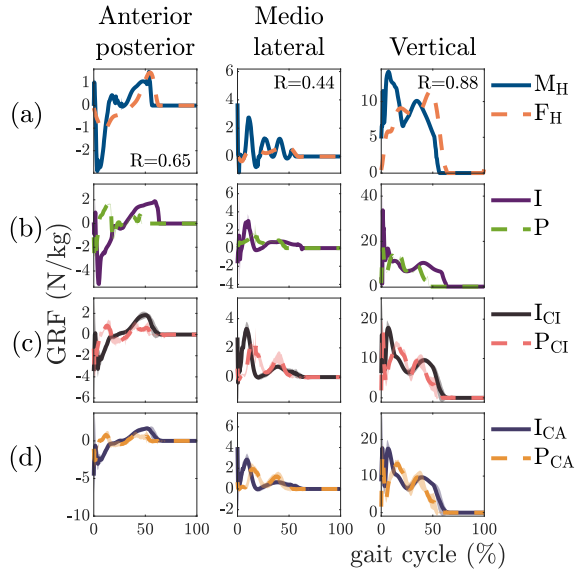

Figure F-6: Average ground reaction forces and standard deviation during a stride of (a) a healthy model (M_H) compared to data from Fukuchi (F_H) [46], and (b) for the intact (I) and prosthetic (P) leg, and (c) for the intact (I_{CI}) and prosthetic (P_{CI}) with inactive CMG, and (d) for the intact (I_{CA}) and prosthetic (P_{CA}) leg with active CMG of the amputee model walking on a flat ground with $1.2\,\mathrm{m/s}$, normalized with the body mass.

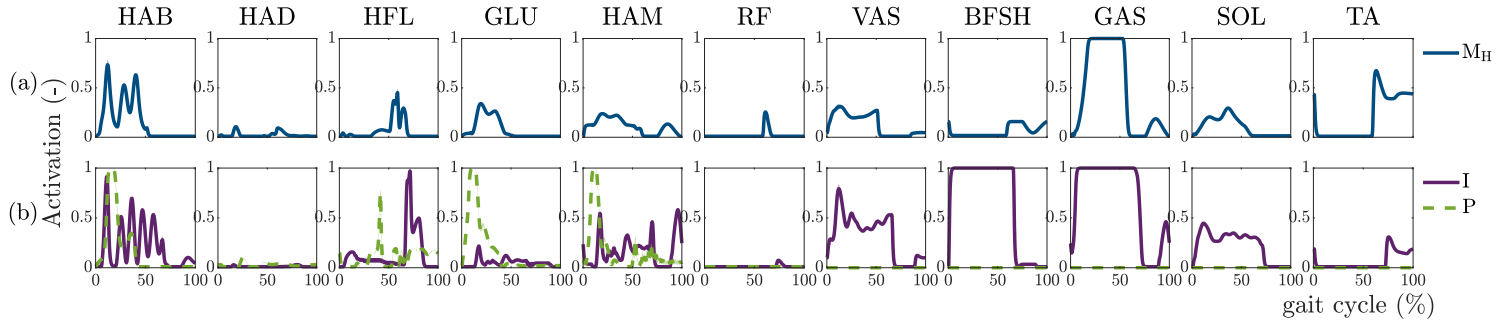

Figure F-7: Average muscle activation levels and standard deviation during a stride of (a) a healthy model (M_H) and (b) the amputee model walking on a flat ground with $0.9\,\mathrm{m/s}$.

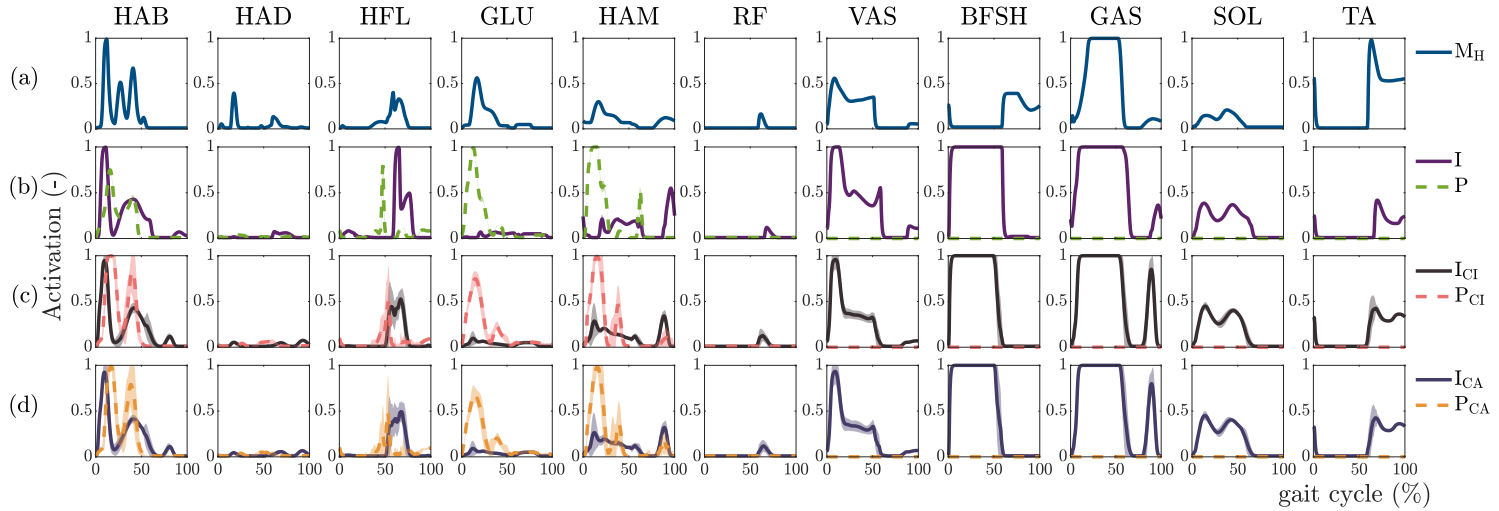

Figure F-8: Average muscle activation levels and standard deviation during a stride of (a) a healthy model (M_H) and (b) for the intact (I) and prosthetic (P) leg, and (c) for the intact (I_{CI}) and prosthetic (P_{CI}) with inactive CMG, and (d) for the intact (I_{CA}) and prosthetic (P_{CA}) leg with active CMG of the amputee model walking on a flat ground with $1.2\,\mathrm{m/s}$.

F-2 Fall prevention using a control moment gyroscope

Fig. F-9 shows the GRF around the moment of tripping and fall prevention.

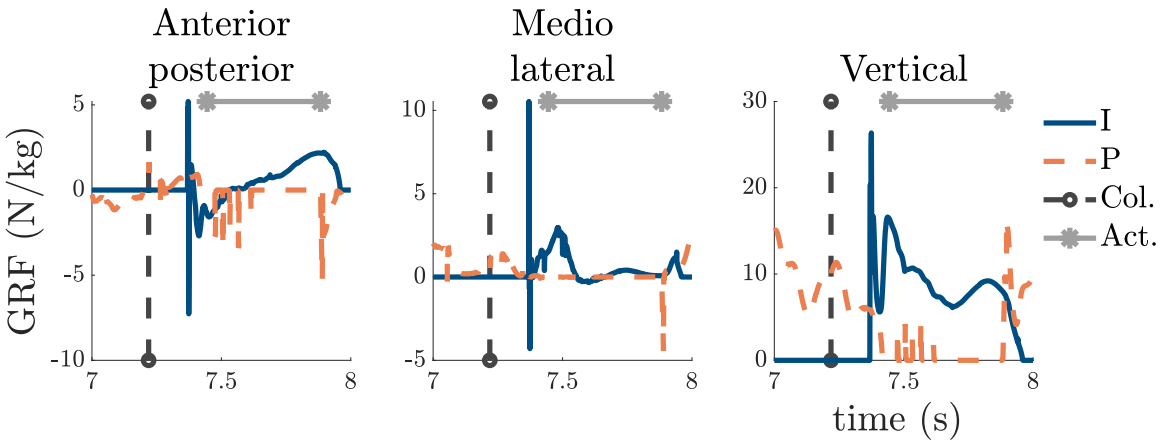

Figure F-9: The ground reaction forces (GRF) for the intact (I) and prosthetic (P) leg around the moment that the amputee model trips. The moment of collision (Col) with the obstacle is around $t = 7.2\,\mathrm{s}$ and the time during which the fall prevention controller is active (Act) is between $t = 7.4\,\mathrm{s}$ and $t = 7.9\,\mathrm{s}$.

Bibliography

[1] K. Ziegler-Graham, E. J. MacKenzie, P. L. Ephraim, T. G. Travison, and R. Brookmeyer, "Estimating the Prevalence of Limb Loss in the United States: 2005 to 2050," *Archives of Physical Medicine and Rehabilitation*, vol. 89, no. 3, pp. 422–429, 2008.

[2] P. F. Pasquina, P. R. Bryant, M. E. Huang, T. L. Roberts, V. S. Nelson, and K. M. Flood, "Advances in amputee care," *Archives of Physical Medicine and Rehabilitation*, vol. 87, no. 3 SUPPL., pp. 34–43, 2006.

[3] R. L. Waters, J. Perry, D. Antonelli, and H. Hislop, "Energy cost of walking of amputees: the influence of level of amputation," *Journal of Bone and Joint Surgery - Series A*, vol. 58, no. 1, pp. 42–46, 1976.

[4] A. M. Boonstra, J. Schrama, V. Fidler, and W. H. Eisma, "The gait of unilateral transfemoral amputees," *Scandinavian Journal of Rehabilitation Medicine*, vol. 26, no. 4, pp. 217–223, 1994.

[5] T. Chin, S. Sawamura, R. Shiba, H. Oyabu, Y. Nagakura, I. Takase, K. Machida, and A. Nakagawa, "Effect of an Intelligent Prosthesis (IP) on the Walking Ability of Young Transfemoral Amputees," *American Journal of Physical Medicine & Rehabilitation*, vol. 82, no. 6, pp. 447–451, 2003.

[6] R. Gailey, K. Allen, J. Castles, J. Kucharik, and M. Roeder, "Review of secondary physical conditions associated with lower-limb amputation and long-term prosthesis use," *Journal of Rehabilitation Research and Development*, vol. 45, no. 1, pp. 15–30, 2008.

[7] M. Bellmann, T. Schmalz, and S. Blumentritt, "Comparative Biomechanical Analysis of Current Microprocessor-Controlled Prosthetic Knee Joints," *Archives of Physical Medicine and Rehabilitation*, vol. 91, no. 4, pp. 644–652, 2010.

[8] J. R. Crenshaw, K. R. Kaufman, and M. D. Grabiner, "Trip recoveries of people with unilateral, transfemoral or knee disarticulation amputations: Initial findings," *Gait and Posture*, vol. 38, no. 3, pp. 534–536, 2013.

[9] M. A. Shandiz, F. Farahmand, and H. Zohour, "Dynamic simulation of the biped normal and amputee human gait," *Mobile Robotics: Solutions and Challenges - Proceedings of the 12th International Conference on Climbing and Walking Robots and the Support Technologies for Mobile Machines, CLAWAR 2009*, pp. 1113–1120, 2010.

[10] A. J. Van Den Bogert, S. Samorezov, B. L. Davis, and W. A. Smith, "Modeling and optimal control of an energy-storing prosthetic knee," *Journal of Biomechanical Engineering*, vol. 134, no. 5, pp. 1–8, 2012.

[11] Y. Geng, P. Yang, X. Xu, and L. Chen, "Design and simulation of active transfemoral prosthesis," *Proceedings of the 2012 24th Chinese Control and Decision Conference, CCDC 2012*, no. 1995, pp. 3724–3728, 2012.

[12] B. E. Lawson, J. Mitchell, D. Truex, A. Shultz, E. Ledoux, and M. Goldfarb, "A robotic leg prosthesis: Design, control, and implementation," *IEEE Robotics and Automation Magazine*, vol. 21, no. 4, pp. 70–81, 2014.

[13] N. Thatte and H. Geyer, "Toward Balance Recovery With Leg Prostheses Using Neuromuscular Model Control," *IEEE Transactions on Biomedical Engineering*, vol. 63, no. 5, pp. 904–913, may 2016.

[14] R. Unal, S. Behrens, R. Carloni, E. Hekman, S. Stramigioli, and B. Koopman, "Conceptual Design of a Fully Passive Transfemoral Prosthesis to Facilitate Energy-Efficient Gait," *IEEE Transactions on Neural Systems and Rehabilitation Engineering*, vol. 26, no. 12, pp. 2360–2366, 2018.

[15] M. Fletcher, "Design and validation of a transfemoral amputee walking model with passive prosthesis swing phase control," Master's thesis, University of Toronto, 2017.

[16] H. Geyer and H. Herr, "A muscle-reflex model that encodes principles of legged mechanics predicts human walking dynamics and muscle activities," *Ieee Transactions on Neural Systems and Rehabilitation Engineering*, vol. 18, no. 3, pp. 1–10, 2010.

[17] D. Lemus, A. Berry, S. Jabeen, C. Jayaraman, K. Hohl, F. C. van der Helm, A. Jayaraman, and H. Vallery, "Controller synthesis and clinical exploration of wearable gyroscopic actuators to support human balance," *Scientific Reports*, vol. 10, no. 1, pp. 1–15, 2020.

[18] S. Jabeen, A. Berry, T. Geijtenbeek, J. Harlaar, and H. Vallery, "Assisting gait with free moments or joint moments on the swing leg," *2019 IEEE 16th International Conference on Rehabilitation Robotics (ICORR)*, pp. 1079–1084, 2019.

[19] S. Song and H. Geyer, "A neural circuitry that emphasizes spinal feedback generates diverse behaviours of human locomotion," *Journal of Physiology*, vol. 593, no. 16, pp. 3493–3511, 2015.

[20] S. Vandaele, "Multi-Body model of the knee prosthesis 3R60," Master's thesis, INSA Rouen, 2003.

[21] MATLAB, "version 9.7.0 (R2019b)," Natick, Massachusetts, 2019.

[22] N. Timmers, "Amputee gait simulation," 2020. [Online]. Available: https://github.com/nathantim/amputee_gait_simulation

[23] S. Jaegers, "The morphology and functions of the muscles around the hip joint after a unilateral transfemoral amputation," Ph.D. dissertation, Rijksuniversiteit Groningen, 1993.

[24] M. Kowal and A. Rutkowska-Kucharska, "Muscle torque of the hip joint flexors and extensors in physically active and inactive amputees," *Biomedical Human Kinetics*, vol. 6, no. 1, pp. 63–68, 2014.

[25] A. Rutkowska-Kucharska, M. Kowal, and S. Winiarski, "Relationship between asymmetry of gait and muscle torque in patients after unilateral transfemoral amputation," *Applied Bionics and Biomechanics*, vol. 2018, 2018.

[26] D. K. Ryser, R. P. Erickson, and T. Cahalan, "Isometric and isokinetic hip abductor strength in persons with above-knee amputations," *Archives of Physical Medicine and Rehabilitation*, vol. 69, no. 10, pp. 840–845, 1988.

[27] F. A. Gottschalk and M. Stills, "The biomechanics of trans-femoral amputation," *Prosthetics and Orthotics International*, vol. 18, no. 1, pp. 12–17, 1994.

[28] H. Geyer, A. Seyfarth, and R. Blickhan, "Positive force feedback in bouncing gaits?" *Proceedings of the Royal Society B: Biological Sciences*, vol. 270, no. 1529, pp. 2173–2183, 2003.

[29] Otto-Bock, "Otto-Bock Image library." [Online]. Available: https://shop.ottobock.us/Image-Library

[30] K. Yin, K. Loken, and M. Van de Panne, "Simbicon: Simple biped locomotion control," *ACM Transactions on Graphics (TOG)*, vol. 26, no. 3, pp. 105–es, 2007.

[31] J. J. Eng, D. A. Winter, and A. E. Patla, "Strategies for recovery from a trip in early and late swing during human walking," pp. 339–340, 1994.

[32] M. J. Pavol, T. M. Owings, K. T. Foley, and M. D. Grabiner, "Mechanisms leading to a fall from an induced trip in healthy older adults," *Journals of Gerontology - Series A Biological Sciences and Medical Sciences*, vol. 56, no. 7, pp. 428–437, 2001.

[33] M. Pijnappels, M. F. Bobbert, and J. H. Van Dieën, "Push-off reactions in recovery after tripping discriminate young subjects, older non-fallers and older fallers," *Gait and Posture*, vol. 21, no. 4, pp. 388–394, 2005.

[34] B. E. Lawson, H. A. Varol, F. Sup, and M. Goldfarb, "Stumble detection and classification for an intelligent transfemoral prosthesis," *2010 Annual International Conference of the IEEE Engineering in Medicine and Biology Society, EMBC'10*, pp. 511–514, 2010.

[35] N. Hansen, "The CMA evolution strategy: a comparing review," in *Towards a new evolutionary computation*. Springer, 2006, pp. 75–102.

[36] B. R. Umberger, "Stance and swing phase costs in human walking," *Journal of the Royal Society Interface*, vol. 7, no. 50, pp. 1329–1340, 2010.

[37] S. M. Jaegers, J. H. Arendzen, and H. J. de Jongh, "Prosthetic gait of unilateral transfemoral amputees: A kinematic study," *Archives of Physical Medicine and Rehabilitation*, vol. 76, no. 8, pp. 736–743, 1995.

[38] E. C. Wentink, E. C. Prinsen, J. S. Rietman, and P. H. Veltink, "Comparison of muscle activity patterns of transfemoral amputees and control subjects during walking," *Journal of NeuroEngineering and Rehabilitation*, vol. 10, no. 1, 2013.

[39] T. S. Bae, K. Choi, D. Hong, and M. Mun, "Dynamic analysis of above-knee amputee gait," *Clinical Biomechanics*, vol. 22, no. 5, pp. 557–566, 2007.

[40] R. E. Seroussi, A. Gitter, J. M. Czerniecki, and K. Weaver, "Mechanical work adaptations of above-knee amputee ambulation," *Archives of physical medicine and rehabilitation*, vol. 77, no. 11, pp. 1209–1214, 1996.

[41] L. Nolan and A. Lees, "The functional demands on the intact limb during walking for active trans-femoral and trans-tibial amputees," *Prosthetics and Orthotics International*, vol. 24, no. 2, pp. 117–125, 2000.

[42] L. Nolan, A. Wit, K. Dudziñski, A. Lees, M. Lake, and M. Wychowañski, "Adjustments in gait symmetry with walking speed in trans-femoral and trans-tibial amputees," *Gait and Posture*, vol. 17, no. 2, pp. 142–151, 2003.

[43] M. Schmid, G. Beltrami, D. Zambarbieri, and G. Verni, "Centre of pressure displacements in trans-femoral amputees during gait," *Gait and Posture*, vol. 21, no. 3, pp. 255–262, 2005.

[44] M. Schaarschmidt, S. W. Lipfert, C. Meier-Gratz, H. C. Scholle, and A. Seyfarth, "Functional gait asymmetry of unilateral transfemoral amputees," *Human Movement Science*, vol. 31, no. 4, pp. 907–917, 2012.

[45] F. Huxham, J. Gong, R. Baker, M. Morris, and R. Iansek, "Defining spatial parameters for non-linear walking," *Gait and Posture*, vol. 23, no. 2, pp. 159–163, 2006.

[46] C. A. Fukuchi, R. K. Fukuchi, and M. Duarte, "A public dataset of overground and treadmill walking kinematics and kinetics in healthy individuals," *PeerJ 6:e4640*, 2018.

[47] X. Drevelle, C. Villa, X. Bonnet, I. Loiret, P. Fodé, and H. Pillet, "Vaulting quantification during level walking of transfemoral amputees," *Clinical Biomechanics*, vol. 29, no. 6, pp. 679–683, 2014. [Online]. Available: http://dx.doi.org/10.1016/j.clinbiomech.2014.04.006

[48] S. Blumentritt, H. W. Scherer, U. Wellershaus, and J. W. Michael, "Design principles, biomechanical data and clinical experience with a polycentric knee offering controlled stance phase knee flexion: a preliminary report," *JPO: Journal of Prosthetics and Orthotics*, vol. 9, no. 1, pp. 18–24, 1997.

[49] J. Beck and J. Czerniecki, "A method for optimization of above-knee prosthetic shank-foot inertial characteristics," *Gait and Posture*, vol. 2, no. 2, pp. 75–84, 1994.

[50] R. W. Selles, J. B. Bussmann, R. C. Wagenaar, and H. J. Stam, "Effects of prosthetic mass and mass distribution on kinematics and energetics of prosthetic gait: A systematic review," *Archives of Physical Medicine and Rehabilitation*, vol. 80, no. 12, pp. 1593–1599, 1999.

[51] M. Telwak, P. Voglewede, and M. B. Silver-Thorn, "Determination of optimal countermass location in active prostheses for transfemoral amputees to replicate sound limb swing," *Journal of Medical Devices, Transactions of the ASME*, vol. 8, no. 4, pp. 1–7, 2014.

[52] B. Moylan, R. Paner, T. Pauley, S. Dilkas, and M. Devlin, "Impact of increased prosthetic mass on gait symmetry in dysvascular transfemoral amputees: A randomized prospective double-blind crossover trial," *Journal of Prosthetics and Orthotics*, vol. 27, no. 2, pp. 63–67, 2015.

[53] J. D. Smith and P. E. Martin, "Short and longer term changes in amputee walking patterns due to increased prosthesis inertia," *Journal of Prosthetics and Orthotics*, vol. 23, no. 3, pp. 114–123, 2011.

[54] A. M. Boonstra, V. Fidler, and W. H. Eisma, "Walking speed of normal subjects and amputees: Aspects of validity of gait analysis," *Prosthetics and Orthotics International*, vol. 17, no. 2, pp. 78–82, 1993.

[55] P. E. Roos, M. P. McGuigan, D. G. Kerwin, and G. Trewartha, "The role of arm movement in early trip recovery in younger and older adults," *Gait and Posture*, vol. 27, no. 2, pp. 352–356, 2008.

[56] S. M. Bruijn, O. G. Meijer, P. J. Beek, and J. H. Van Dieën, "The effects of arm swing on human gait stability," *Journal of Experimental Biology*, vol. 213, no. 23, pp. 3945–3952, 2010.

[57] B. R. Umberger, K. G. Gerritsen, and P. E. Martin, "A model of human muscle energy expenditure." *Computer methods in biomechanics and biomedical engineering*, vol. 6, no. 2, pp. 99–111, 2003.

Glossary

List of Acronyms

3mE	Mechanical, Maritime and Materials Engineering
DCSC	Delft Center for Systems and Control
TU Delft	Delft University of Technology
TF	trans-femoral
AK	above-knee
CE	contractile element
SE	series element
PE	parallel element
BE	buffer element
MTU	muscle-tendon unit
HAB	hip abductors
HAD	hip adductors
HFL	lumped hip flexors
GLU	glutei
HAM	hamstrings
RF	rectus femoris
VAS	vastii
BFSH	short head of biceps femoris
GAS	gastrocnemius
SOL	soleus
TA	tibialis anterior
CMG	control moment gyroscope
CMAES	covariance matrix adaption evolution strategy
DOF	degree of freedom
FD	forward dynamic
MTC	minimum toe clearance
HAT	head, arms, and torso
CoT	cost of transport
TVC	target velocity cost
STC	stop torque cost
COM	center of mass
ASI	absolute symmetry index
TLA	target leg angle
GRF	ground reaction forces
GM	gimbal motor
ICR	instantaneous center of rotation